Evaluation of Mixtures and Pavement Performance for Rehabilitation Methods

FINAL REPORT

Mohammad Rahmani, Gabriel Nsengiyumva, Yong-Rak Kim

Zachry Department of Civil and Environmental Engineering

Texas A&M University

College Station, Texas

and

Jiong Hu

Department of Civil and Environmental Engineering

University of Nebraska-Lincoln

Omaha, Nebraska

Sponsored By

Nebraska Department of Transportation and U.S. Department of Transportation Federal Highway Administration

September 2020

NEBRASKA

Good Life. Great Journey.

DEPARTMENT OF TRANSPORTATION

TECHNICAL REPORT DOCUMENTATION PAGE

1. Report No. SPR-P1(19) M084	2. Government Accession No.	3. Recipient's Catalog No.
4. Title and Subtitle Evaluation of Mixtures and Pavement Performance for Rehabilitation Methods		**5. Report Date** September 15, 2020 **6. Performing Organization Code**
7. Author(s) Mohammad Rahmani, Gabriel Nsengiyumva, Yong-Rak Kim, and Jiong Hu		**8. Performing Organization Report No.**
9. Performing Organization Name and Address **Prime Organization:** Department of Civil and Environmental Engineering University of Nebraska-Lincoln Omaha, Nebraska 68182 **Subaward Organization:** Zachry Department of Civil and Environmental Engineering Texas A&M University College Station, Texas 77843-3136		**10. Work Unit No.** **11. Contract**
12. Sponsoring Agency Name and Address Nebraska Department of Transportation Research Section 1400 Hwy 2 Lincoln, NE 68502		**13. Type of Report and Period Covered** Final Report, 07/01/2018 – 09/15/2020 **14. Sponsoring Agency Code**
15. Supplementary Notes		

16. Abstract

Pavement rehabilitation practice involves milling an asphalt surface and placing a new layer. The incorporation of reclaimed asphalt pavement (RAP) mixtures brings cost savings and preserves the environment and natural resources. However, the use of recycled materials can compromise pavement performance, in particular, RAP can contribute to cracking because the mixtures with recycled materials become more brittle. In Nebraska, pavement rehabilitation has mostly been conducted by milling old 4-in. asphalt surface and placing a new 4-in. layer. Due to the potentially increased use of RAP mixtures for pavement rehabilitation, it is necessary to look into potential applications of RAP-induced overlay configurations that can save costs without compromising pavement performance. Toward that end, this research project selected six overlay mixtures containing RAP in different qualities. Mixtures were tested to identify mechanical and fracture properties in low and intermediate temperatures. Using these mixture properties, the thermo-mechanical behavior of asphalt pavements was predicted by conducting finite element simulations incorporated with cohesive zone fracture for both thermal cracking and reflective cracking. A total of seven overlay configurations (a seventh tested a 2-in. layer for comparison) were considered and compared. Pavement performance and predicted life from the finite element modeling were then used to conduct life cycle cost analyses (LCCA). Regarding load-induced reflective cracking, test and modeling results indicated that the conventional overlay practice with SPR mixture would perform similar with the case of 4.0-in. SLX and generally better than other cases considered in this study. In terms of thermally-induced cracking, pavement performance simulation results showed that the case with 4-in. SLX was the best, and cases with SLX on top generally perform better than cases with SPR. The overlays made with poor-quality RAP showed significant damage increase compared to those made with good-quality RAP. This implies a careful use and management of RAP is desired to sustain long-term pavement performance. LCCA based on reflective cracking results indicated that the 4.0-in. SPR is the most economical strategy compared to other alternatives considered in this study in terms of the agency costs. It can also be noted that the combination of 2-inch SRM + 2-inch SLX is a good option for colder regions in Nebraska, as the combined overlay showed almost similar reflective cracking behavior to and better in thermal cracking resistance than the conventional 4.0-in. SPR rehabilitation.

17. Key Words	18. Distribution Statement		
Pavement Rehabilitation, Reclaimed Asphalt Pavement, Finite Element Modeling, Performance Prediction, Thermal Cracking, Reflective Cracking, Life Cycle Cost Analysis.	No restrictions. This document is available through the National Technical Information Service. 5285 Port Royal Road Springfield, VA 22161		
19. Security Classification (of this report)	**20. Security Classification**	**21. No. of Pages**	**22. Price**
Unclassified	Unclassified	74	

Table of Contents

List of Figures

PAGE

List of Tables

PAGE

Acknowledgments

The authors thank the Nebraska Department of Transportation (NDOT) for the financial support needed to complete this study. In particular, the authors thank the NDOT Technical Advisory Committee (TAC) for their technical support and invaluable discussions/comments.

Disclaimer

The contents of this report reflect the views of the authors, who are responsible for the facts and the accuracy of the information presented herein. This document is disseminated under the sponsorship of the Department of Transportation University Transportation Centers Program, in the interest of information exchange. The U.S. Government assumes no liability for the contents or use thereof.

Abstract

Pavement rehabilitation practice involves milling an asphalt surface and placing a new layer. The incorporation of reclaimed asphalt pavement (RAP) mixtures brings cost savings and preserves the environment and natural resources. However, the use of recycled materials can compromise pavement performance, in particular, RAP can contribute to cracking because the mixtures with recycled materials become more brittle. In Nebraska, pavement rehabilitation has mostly been conducted by milling old 4-in. asphalt surface and placing a new 4-in. layer. Due to the potentially increased use of RAP mixtures for pavement rehabilitation, it is necessary to look into potential applications of RAP-induced overlay configurations that can save costs without compromising pavement performance. Toward that end, this research project selected six overlay mixtures containing RAP in different qualities. Mixtures were tested to identify mechanical and fracture properties in low and intermediate temperatures. Using these mixture properties, the thermo-mechanical behavior of asphalt pavements was predicted by conducting finite element simulations incorporated with cohesive zone fracture for both thermal cracking and reflective cracking. A total of seven overlay configurations (a seventh tested a 2-in. layer for comparison) were considered and compared. Pavement performance and predicted life from the finite element modeling were then used to conduct life cycle cost analyses (LCCA). Regarding load-induced reflective cracking, test and modeling results indicated that the conventional overlay practice with SPR mixture would perform similar with the case of 4.0-in. SLX and generally better than other cases considered in this study. In terms of thermally-induced cracking, pavement performance simulation results showed that the case with 4-in. SLX was the best, and cases with SLX on top generally perform better than cases with SPR. The overlays made with poor-quality RAP showed significant damage increase compared to those made with good-quality RAP. This implies a careful use and management of RAP is desired to sustain long-term pavement performance. LCCA based on reflective cracking results indicated that the 4.0-in. SPR is the most economical strategy compared to other alternatives considered in this study in terms of the agency costs. It can also be noted that the combination of 2-inch SRM + 2-inch SLX is a good option for colder regions in Nebraska, as the combined overlay showed almost similar reflective cracking behavior to and better in thermal cracking resistance than the conventional 4.0-in. SPR rehabilitation.

Chapter 1 Introduction

About 75% of the pavement 3R (resurfacing/restoration/rehabilitation) practices in Nebraska is done by milling old 4-inch asphalt surface and placing a new 4-inch layer. Another 10% is a deeper replacement such as 5-inch mill and fill or 6-inch mill and fill. Traditionally, the Nebraska Department of Transportation (NDOT) has used one asphalt mixture for the 4-inch strategy (i.e., previously 4-inch of the SP4 mix, now 4-inch of the SPR mix which is cheaper and has higher RAP content and stiffness). For deeper rehabilitation purposes, NDOT has been using a combination of SRM with SPR or SLX. SRM usually allows 35% to 65% RAP (reclaimed asphalt pavement) with a coarser mix gradation so that high stiffness can be achieved. The incorporation of high-RAP brings cost savings and preserves the environment and natural resources (due to more recycling).

Because specific combined layer configurations between SRM, SPR, and SLX can provide cost savings due to the use of more recycled materials, while not compromising pavement performance, NDOT has been interested in investigating if alternative overlay configurations (e.g., 3-in. SRM and 1-in. SLX, 2.5-in. SRM and 1.5-in. SPR, etc.) can be used for the 4-in. rehabilitation practice, in addition to deeper rehabilitation strategies using SRM. However, it is not certain if different layer combinations which include SRM would be more prone to top-down thermal cracking or bottom-up reflective cracking compared with the single 4-in. SPR mix approach due to the higher RAP content in SRM.

To improve pavement engineering practices in Nebraska, there is a clear need to look into the feasibility and potential applications of overlay configurations with more economical mixes, and this requires research efforts to address several important questions, including (1) if the new layer configurations including SRM and SLX in pavements perform adequately compared with the conventional 4-in. mill and fill by SPR, in particular, with resistance to cracking and (2) if the new layer configurations can save life cycle costs (LCC) compared with the conventional 4-in. mill and fill rehabilitation practice by SPR.

1.1. Research objective and scope

The main objective of this research is to test typical asphalt mixtures and use their mechanical and fracture properties to predict pavement performance and LCCA when they are used in different

rehabilitation practices in Nebraska pavements. Toward that end, this research project selected six overlay mixtures containing RAP in different qualities. Mixtures were tested to identify mechanical and fracture properties in low and intermediate temperatures. Using these mixture properties, thermo-mechanical behaviors of asphalt pavements were predicted by conducting finite element simulations incorporated with cohesive zone fracture for both thermal cracking and reflective cracking. A total of seven overlay configurations (a seventh tested a 2-in. layer for comparison) were considered and compared. Pavement performance and predicted life from the finite element modeling were then used to conduct life cycle cost analyses (LCCA). Overall, the outcomes of this research can help the NDOT by providing a comparative understanding of the performance and durability of asphalt mixture combinations to support decision-making. Ultimately, this research can contribute to a more engineered and better design of pavement structures and the use of paving materials more economically by providing core information and practical insights.

1.2. Organization of this report

This report includes six chapters. Following this introduction, Chapter 2 summarizes the literature on the modeling of pavements when considering thermal and mechanical loads. Chapter 3 presents the laboratory tests of state mixes (SPR, SRM, and SLX) with different qualities of RAP to identify RAP-dependent mixture properties at low and intermediate temperatures, including the dynamic modulus test and semicircular bend (SCB) fracture test. Chapter 4 describes the finite element modeling and simulations of different pavement structures. The simulation results of various alternatives for overlay configurations are also discussed in this chapter. Chapter 5 presents the LCCA of pavements resulting from different rehabilitation alternatives. Finally, Chapter 6 provides a summary of the findings and offers conclusions for the study.

Chapter 2 Background

The intrinsic heterogeneous nature of asphalt mixtures makes their cracking behavior challenging to address. Several studies have been conducted on pavement performance analysis and prediction. While many researchers focus more on experimental approaches to address pavement performance at the mixture level, there are many who have attempted to analyze the pavements' cracking behaviors computationally by incorporating continuum and fracture mechanics.

To investigate the economic benefits of different alternatives in pavement construction and rehabilitation, life cycle cost analysis (LCCA) has been widely used in academia and industry. Considering major activities of each alternative, one can analyze the agency and user cost of the pavement construction projects over a long period of time.

In the following chapter, selected research studies on pavement performance analysis and LCCA are reviewed.

2.1. Pavement performance analysis and prediction

Mechanistic-Empirical Pavement Design Guide (MEPDG) is a widely used tool to design pavements in an effectively reversed way compared to the conventional methods. It was designed to update the AASHTO Guide for Design of Pavement Structures. Two main parts associated with MEPDG include a focus on physical causes of distresses in pavement structures, which is the "mechanistic" part, and using observed performance to determine relationships between distresses and their causing key factors, which is the "empirical" part. The term "reversed" is used to address the fact that the design of pavement in MEPDG is initially assumed on a trial basis. The mechanistic approach is used to analyze the response of the pavement to given traffic and climate inputs. The result of this process shows the level of damage that the trial pavement design can sustain over time. Table 2.1 presents some of the studies carried out using MEPDG.

Overlays with a thickness over 50.8 mm (2-inches) were considered for MEPDG simulations, while pavement structures with 25.4 mm (1-inch) thin overlay were simulated in Louisiana. Rutting, cracking, and roughness, calculated by the International Roughness Index (IRI), were predicted as major distresses using MEPDG.

Table 2.1 Summary of the studies using MEPDG for the performance prediction of overlays

State	Performance indicator	Overlay thickness (mm)	Reference
South Dakota	• Longitudinal cracking • Transverse cracking • Fatigue cracking • Rutting • IRI	50.8-127.0	Hoerner et al. (2007)
Tennessee	• Rutting • IRI	108.0-343.0	Zhou et al. (2013)
Louisiana	• Fatigue cracking • Rutting • IRI	25.4-121.9	Wu et al. (2008)
Minnesota	• Transverse cracking	50.8	Johanneck et al. (2011)
Utah	• Fatigue cracking • Rutting • IRI	45.7-58.4	Guthrie and Butler (2011)
Washington	• Fatigue cracking • Rutting • Reflective cracking	50.8	Khazanovich et al. (2013)
Alberta (Canada)	• Fatigue cracking • Rutting • IRI	50.0-120.0	Norouzi et al. (2014)
IRI: International Roughness Index			

An integrated, performance-based pavement design tool called “FlexPAVE system” was introduced by Wang et al. (2018, 2020) at NC State University. This system includes a suite of tools to link material tests (“asphalt mixture performance tester” or AMPT), mixture analysis (FlexMAT software), and pavement analysis (FlexPAVE software), as shown in Figure 2.1. The system ultimately links to mixture design, performance specifications, and pavement design; a process which is called performance-engineered mixture design (PEMD).

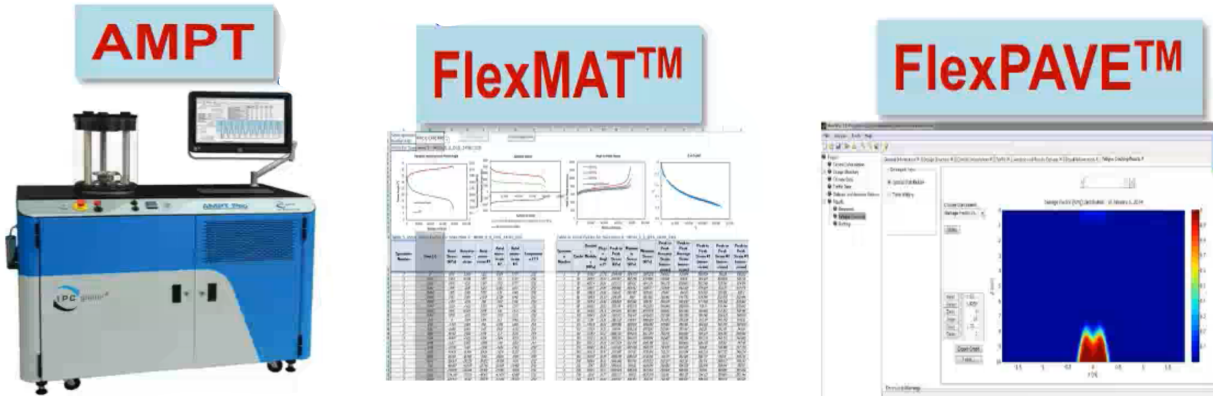

(a) (b) (c)

Figure 2.1. FlexPAVE system tools for: a) material testing, b) material analysis, and c) pavement analysis.

In PEMD, pavement performance is a function tied to materials properties, structural design, and climate. The PEMD-predictive estimates the pavement life in years through a function to predict pavement performance using measurable volumetric quantities. Figure 2.2 shows the performance of a mixture in a specific pavement design and its estimated life contour using PEMD-predictive.

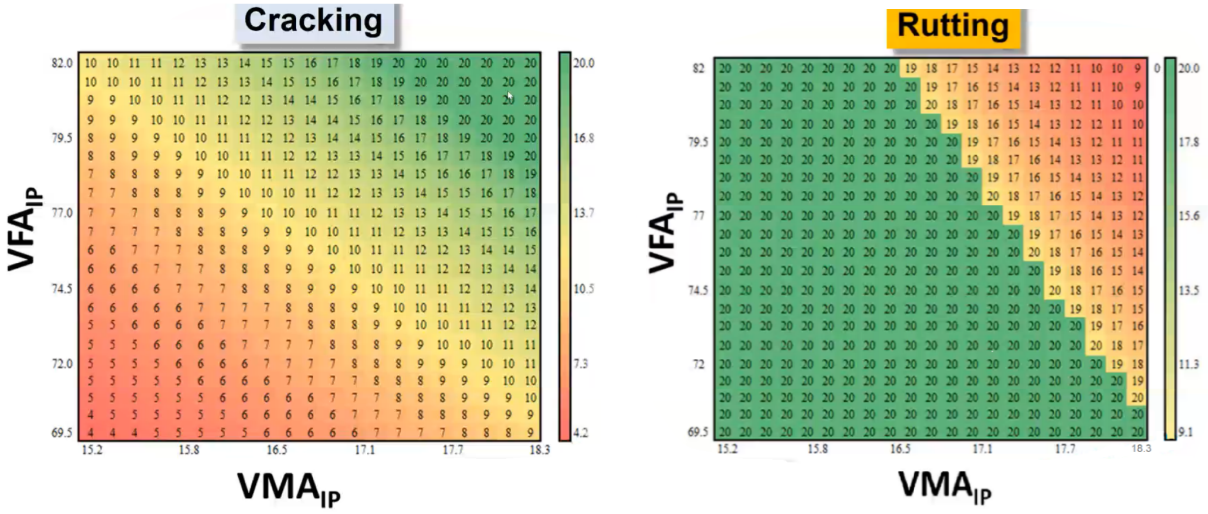

(a) (b)

Figure 2.2. PEMD-predictive results (in years) for: (a) cracking, and (b) rutting.

Finite element modeling (FEM) is a common tool for structural performance analysis, which, compared to MEPDG, can provide more flexibility in selecting geometries, boundary conditions, and choosing materials in the analysis.

To computationally model the fracture behavior of asphalt materials using FEM, cohesive zone modeling (CZM) has recently captured researchers' interests. Li et al. (2004) applied CZM to simulate the fracture response of asphalt concrete numerically. Kim et al. (2005) used a micromechanical nonlinear viscoelastic cohesive zone in their finite element model to predict damage-induced mechanical response of asphalt mixtures. Kim et al. (2007) used a nonlinear viscoelastic cohesive zone model to represent the rate-dependent damage response of asphalt materials. Lutif et al. (2010) used a two-way multiscale model with cohesive zone fracture to take into account the inherited heterogeneity, inelasticity, and damage accumulation of asphalt materials. Aragão and Kim (2012) investigated mode-I (opening) fracture behavior of bituminous mixtures through an experimental-numerical study using 2-D SCB test geometry and showed the rate dependency of cohesive zone fracture properties. Zare et al. (2018) integrated a two-way linked multiscale method incorporated with cohesive zone fracture, with nanomechanical tests to model highly heterogeneous multiphase media. Rodrigues et al. (2019) used extrinsic nonlinear viscoelastic cohesive zone model to efficiently predict nucleation, initiation, and propagation of cracks in fine aggregate matrix (FAM) bituminous materials. Baek and Al-Qadi (2009) investigated reflective cracking of HMA overlays using finite element models that consisted of a 57-mm-thick overlay over a 200-mm-thick joint plain concrete pavement. As shown in Figure 2.3 cohesive elements were embedded over the transverse joints, where reflective cracking potentially occurred in HMA overlays.

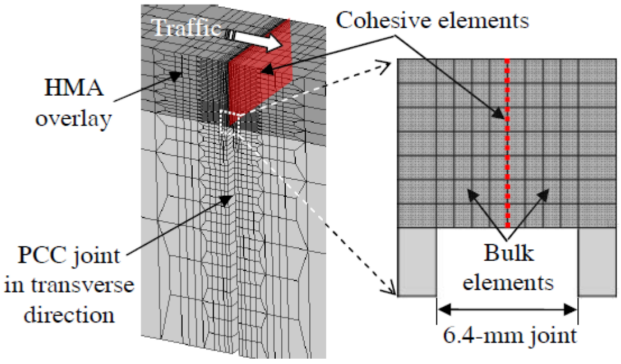

Figure 2.3. Finite element modeling of reflective cracking [Baek and Al-Qadi (2009)].

In 2012, researchers at Texas A&M University developed a FEM tool in which the non-linear thermo-viscoelasticity, thermo-viscoplasticity, and thermo-viscodamage were coupled to solve for more challenging and sophisticated problems and address many complexities associated with asphalt concrete material. The FEM tools were called the Pavement Analysis using Nonlinear Damage Approach (PANDA; You et al. 2012). The PANDA software brought significant improvements regarding the use of material characteristics and non-linear FE method for analysis and design of pavement structures. The aging and healing responses of asphalt concrete (AC) are also incorporated in PANDA (Darabi et al. 2011, 2012, 2013).

In 2016, Shakiba et al. introduced realistic tire-pavement interaction and contact stresses into PANDA, as shown in Figure 2.4.

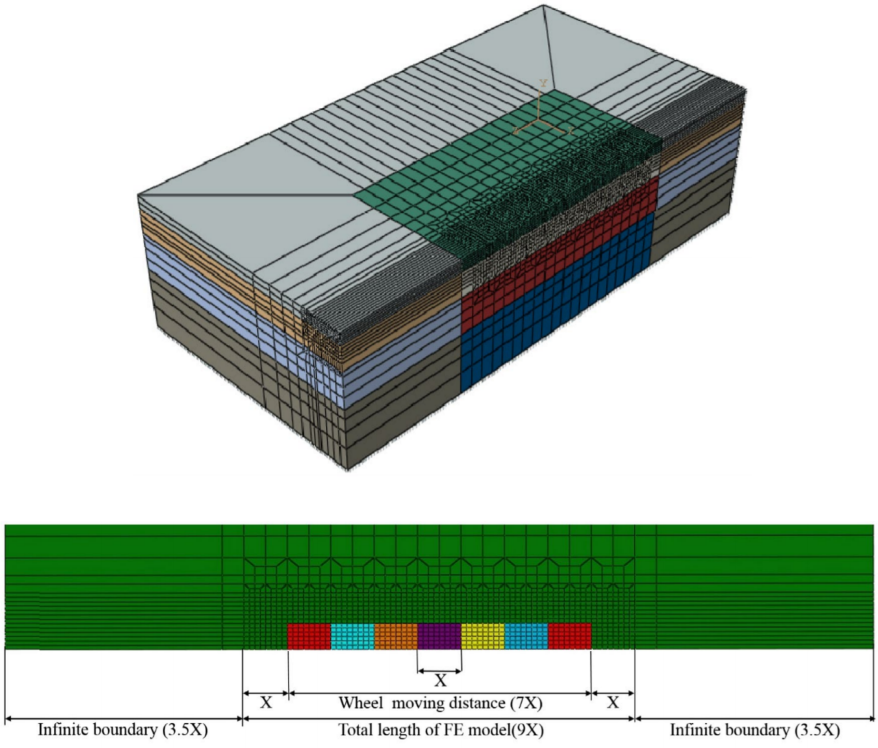

Figure 2.4. Pavement model in PANDA software: up) 3D, and bottom) 2D models.

In 2018, Zare and Kim developed a user-friendly software: Pavement-Simulator. It generates a simplified 2-D FE model of pavements for simulating various distresses including cracking within layers and debonding between layers. It can simulate crack propagation of an overlay using embedded cohesive elements while it considers the time-dependent behavior of

layers, bonding (or friction) condition between layers, and presence of pre-existing distresses within layers such as joints and/or cracks. Pavement-Simulator facilitates the performance analysis through its user-friendly interface and takes into account the viscoelastic AC mixture properties and cohesive zone fracture with a damage evolution law. Figure 2.5 shows an example of a 3-layer pavement structure subjected to a cyclic tire loading and cohesive zone fracture due to the loading.

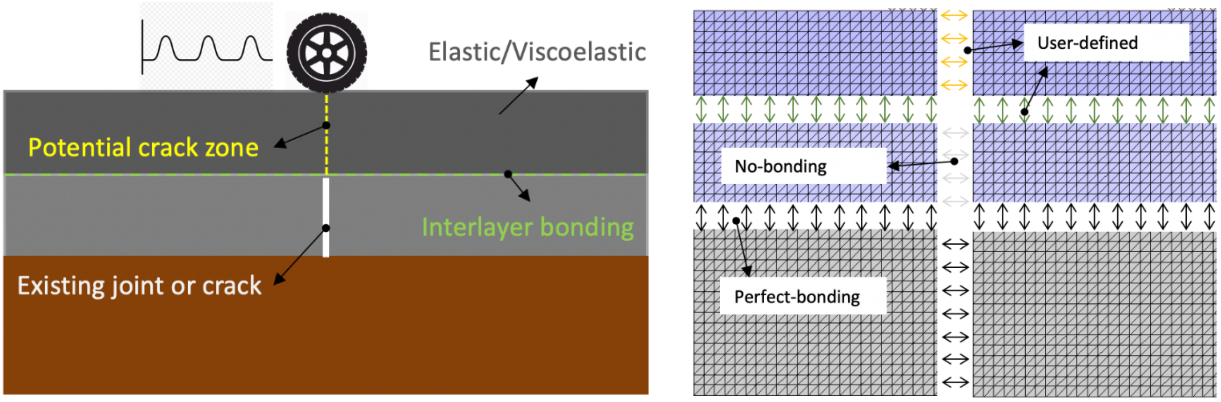

(a) (b)

Figure 2.5. Pavement-Simulator FEM tool: a) physical description, and b) mesh and layers bonding.

Many researchers have made great efforts to investigate the thermal cracking behavior of asphaltic pavement structures. To represent the behavior of pavement structures, such as cracking under thermal loads, it is necessary to examine the thermal cracking mechanism and to incorporate appropriate constitutive material models into these structural mechanistic models.

Thermal cracking generally depends on both the magnitude of the low temperature experienced and the cooling rates. Mukhtar and Dempsey (1996) investigated the thermal cracking mechanism of the overlay of asphalt concrete (AC) on Portland cement concrete (PCC) under seasonal temperature changes and daily temperature cycles, as shown in Figure 2.6.

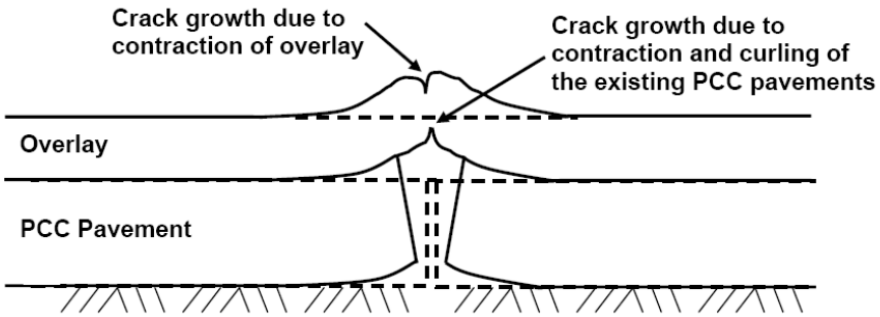

Figure. 2.6. Crack propagation in the overlay due to temperature changes [Mukhtar and Dempsey (1996)].

As depicted in the above figure, they reported that due to the temperature cooling down in the evening, the temperature on the surface of the slab is cooler than the bottom of the slab because the effect of the temperature decrease reaches the top of the slab first. The top of the slab contracts causing it to curl upwards and generating tensile stress in the overlay at the top of the joint. Potentially, the combination of the PCC slabs and overlay movements due to temperature differences can cause cracking to initiate from both the top and the bottom of the overlay.

Selvadurai et al. (1990) conducted the transient stress analysis of a multilayer pavement structure subjected to heat conduction and associated thermal-elastic effects by the cooling of its surface using finite element analysis. They analyzed the pavement structure behavior at low temperature considering three specific effects: the thickness of the cracked existing asphalt layer, surface crack depth, and the presence of cracks at both the existing asphalt layer and newly paved asphalt layers.

To predict and characterize the thermal cracking behavior, the current Superpave specifications and the mechanistic-empirical pavement design guide (MEPDG) are based on the creep and strength data for both asphalt binders and asphalt mixtures. For asphalt binders, two laboratory instruments were developed during the Strategic Highway Research Program (SHRP) to investigate the low-temperature behavior of asphalt binders: the bending beam rheometer (BBR) and the direct tension tester (DTT). For asphalt mixtures, one laboratory-testing device was developed: indirect tension (IDT) tester. The critical temperature is determined at the intersection between the tensile strength-temperature curve and the thermal stress temperature curve. This approach is used in the thermal cracking (TC) model, which has been implemented in the MEPDG.

The TC model is based on the theory of viscoelasticity, which mechanically predicts thermal stress as a function of time and depth in pavements based on pavement temperatures, which are calculated using local air temperatures. However, several limitations in the TC model have been identified, such as the use of the simple, phenomenological crack evolution law to estimate the crack growth rate, using test results obtained from the Superpave IDT test, which does not accurately identify fracture properties. Besides, the TC model does not consider crack developments related to vehicle loads and environmental conditions; thus, this model cannot fully reflect fracture processes in the mixtures and pavements that are subjected to traffic loading, moisture damage, and low-temperature conditions.

Dave et al. (2007) carried out research on modeling of reflective and thermal cracking of asphalt concrete using the cohesive zone model. They investigated the pavement behavior of an intermediate climate region located at U.S. State Highway 36 near Cameron, Missouri. Although they concluded that the finite element simulations with the cohesive zone model could predict cracking behavior quantitatively, the model validation with field measurement has not yet been provided for use in the study.

Dave and Buttlar (2010) extended their previous study to investigate the thermal reflective cracking of asphalt concrete overlays over PCC and rubblized slab considering different types of mixtures, overlay thicknesses, and joint spacings of PCC. The authors used the same modeling technique representing thermal cracking behavior as their previous study, which was cohesive zone fracture modeling as shown in Figure 2.7. Based on their findings, the overlays over the PCC joints showed bottom-up cracking, while overlays over the rubblized slab revealed top-down cracking. However, this may not be accurate because the pavement response to the thermal loading may have been affected by the material properties (i.e., thermal coefficient of asphalt concrete, PCC slab, rubblized slab, and fracture properties of asphalt concrete) as well as the geometry of pavement structures.

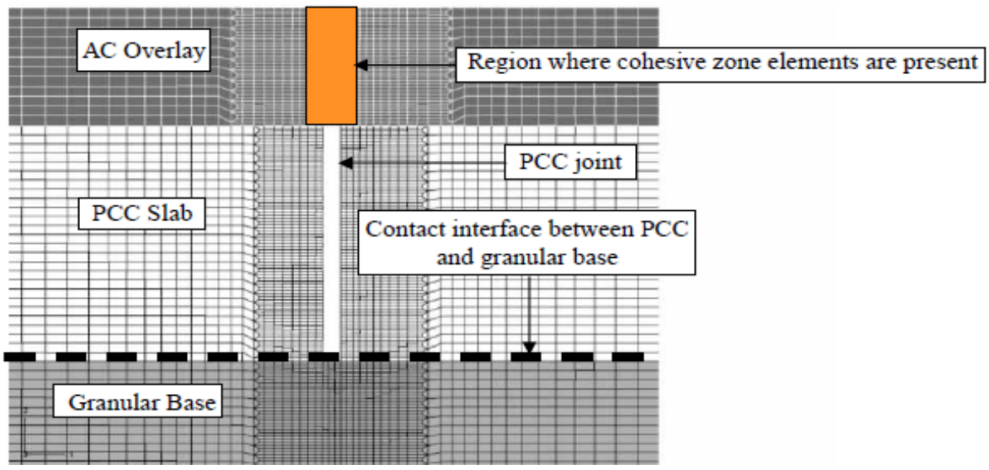

Figure 2.7. FE modeling of thermal cracking [Dave and Buttlar (2010)].

Kim and Buttlar (2009) examined the low-temperature cracking behavior of airport pavements under daily temperature change using cohesive zone modeling. To this end, they performed creep compliance tests, indirect tensile tests (IDT), and disk-shaped compact tension (DC[T]) tests to obtain numerical model inputs, such as the viscoelastic and fracture properties of asphalt concrete at low temperature. They reported that two-dimensional fracture models could successfully simulate the crack initiation and crack propagation. Furthermore, the large aircraft loading, coupled with thermal loading, had an adverse influence on pavement cracking behavior. However, although the fracture properties are temperature dependent, the fracture properties of -20C were used in their models.

Souza and Castro (2012) studied the mechanical response of thermo-viscoelastic pavements, considering temperature effect. They used an in-house finite element code, which incorporated the thermo-viscoelastic constitutive model, to investigate the effects of mechanical tire loading, thermal expansion or contraction, and thermo-susceptibility of viscoelastic asphalt materials on the overall pavement responses. Through the various sensitivity analyses, they reported that the deformation and stresses were considerably affected by both thermal deformation and the thermo-susceptibility of the viscoelastic material, individually and together. Figure 2.8 shows their FEM model and its results on temperature dependent mechanical response of material under tire pressure.

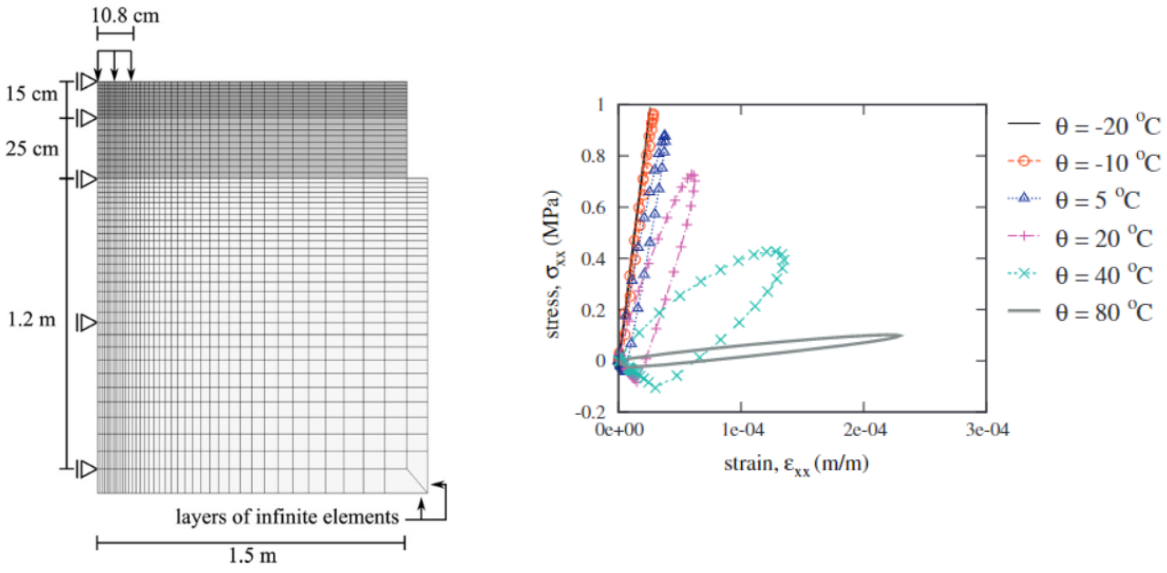

(a) (b)

Figure 2.8. FE modeling of pavement [Souza and Castro 2012]: a) FEM mesh, and b) mechanical response of materials in different temperatures.

Ban et al. (2013) carried out laboratory tests and finite element simulations to model thermally induced reflective cracking in composite pavements. They used cohesive elements in their FEM models to evaluate the damage behavior of pavement structure during a single cooling event. They did a parametric study on material properties and pavement geometry to find sensitive factors in overall pavement performance at low temperature. Figure 2.9 shows the horizontal stress developed at top and bottom of the AC overlay when using different damage parameters.

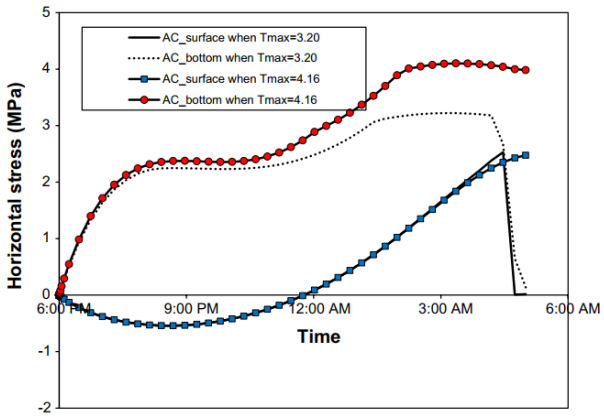

Figure 2.9. Horizontal stresses in the pavement overlay during a single cooling event.

2.2. Life cycle cost analysis (LCCA) of pavements

Life cycle cost analysis evaluates the total economic worth of a project over its lifetime. It considers initial construction cost, service cost, preservative maintenance cost, operating cost, and disposal cost. It helps to determine the most cost-effective option among many alternatives. For a pavement construction or rehabilitation project, it also considers the user cost. All agency and user costs are usually discounted and totaled to a present-day value which is also known as net present value (NPV).

Among many platforms by which LCC can be computed, two programs are widely used. RealCost 2.5 developed by the Federal Highway Administration (FHWA), and PAVExpress developed by National Asphalt Pavement Association (NAPA). Figure 2.10 shows the user interface of these two software.

(a)

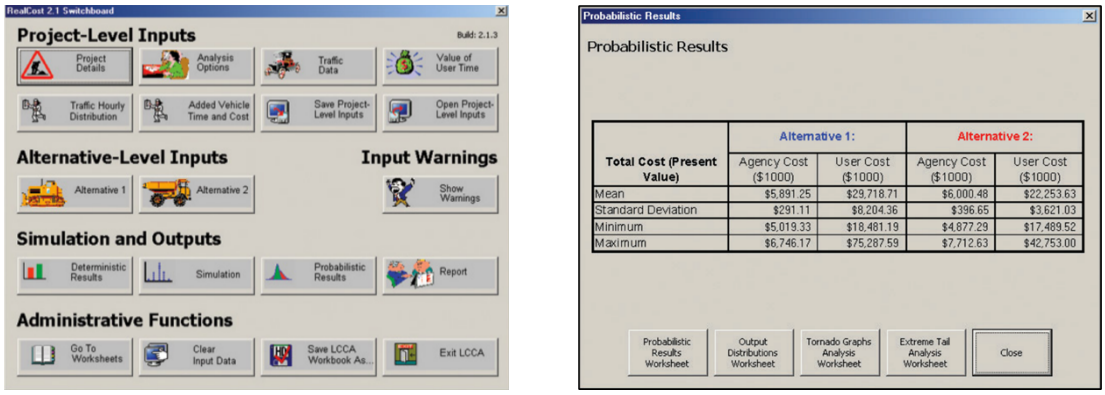

(b)

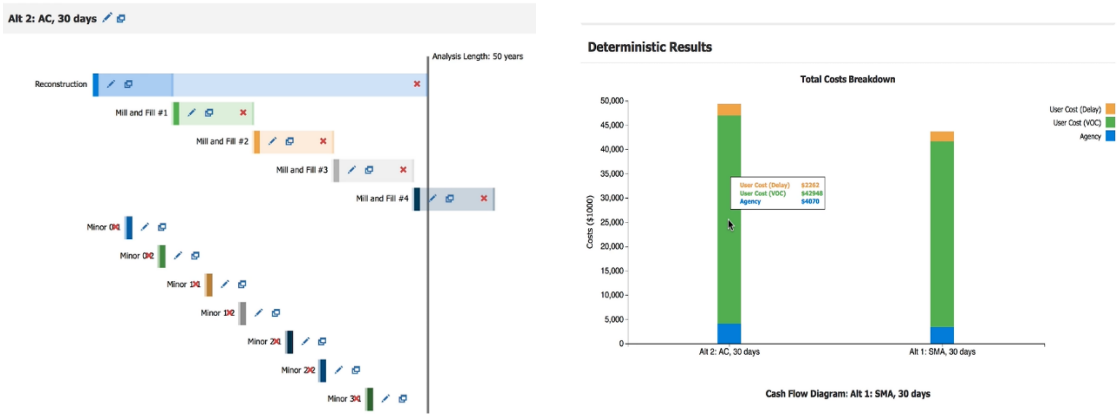

Figure 2.10. LCCA software: a) FHWA's RealCost 2.5, and b) NAPA's PAVExpress.

In 2014, Aurangzeb and Al-Qadi conducted research for Illinois DOT in which they used LCCA to analyze the economic and environmental feasibility of using high RAP content in pavements for a period of 45 years. They used FHWA's software, RealCost 2.5, which considers both agency and user costs. The agency costs in their study were calculated based on initial construction, maintenance, and rehabilitation activities. They calculated user costs based on traffic data. The deterministic life cycle costs for mixture alternatives are shown in Figure 2.11.

Cost Item	Control	Mix with 30% RAP	Mix with 40% RAP	Mix with 50% RAP
Agency ($/mi)	785,514	729,215	710,449	691,683
User ($/mi)	779,396	779,396	779,396	779,396
Total life-cycle ($/mi)	1,564,909	1,508,612	1,489,846	1,471,080
Net savings compared with control ($/mi)	na	56,297	75,063	93,829

(a)

Cost Item	Control	Mix with 30% RAP	Mix with 40% RAP	Mix with 50% RAP
Initial construction ($/mi)	580,321	524,024	505,258	486,492
Maintenance ($/mi)	205,193	205,193	205,193	205,193
Total ($/mi)	785,514	729,216	710,451	691,685

(b)

Figure 2.11. LCCA for pavement project [Aurangzeb et al (2014)]: a) LCC for mix alternatives, and b) total NVP.

Aurangzeb and Al-Qadi (2014) also considered different scenarios for pavement performance level and calculated the present value of agency cost and total cost over the lifetime of the pavement for each scenario. The major limitation of their work was that the lifetime was presumed for each case and was not calculated. Figure 2.12 shows the results of their study.

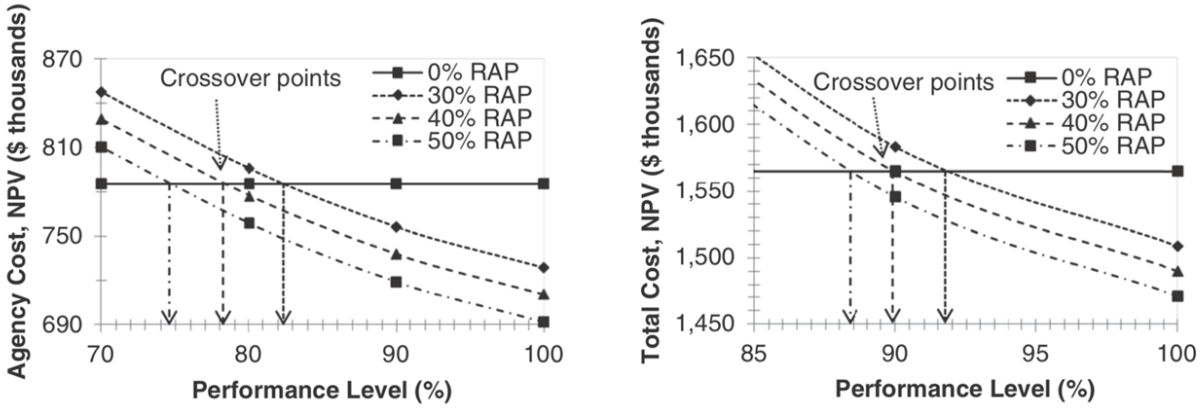

Figure 2.12. Agency cost and total cost of the projects based on performance level [Aurangzeb et al (2014)].

In 2011, Kholsa and Visintine carried out a life cycle cost analysis of pavement projects for North Carolina DOT. They used artificial intelligence-based models to estimate fatigue life of different pavement systems and to estimate their initial service life, which is a key factor in LCCA, as shown in Figure 2.13. Based on their findings, mixtures containing 30% RAP and 40% RAP, have a present worth that is 19% and 35% less than the virgin mixture, respectively.

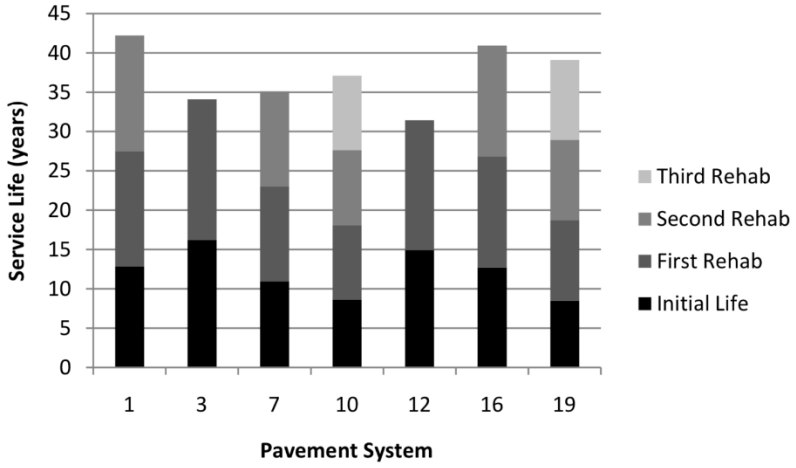

Figure 2.13. Estimate service life of the pavements [Visintine et al. (2011)].

In 2019, Qiao et al. carried out performance analysis and LCCA for pavements with 40% RAP and different structures to evaluate their economic benefits. Based on their results, the agency costs of hot mix asphalt (HMA) with 40% RAP are less than virgin HMA for all structures, due to its material saving in the production phase. The cost reduction ranges between 0.2%–18.3%. Although it requires more treatment for thermal cracking, the incurred additional maintenance costs were less than the production cost savings. Figure 2.14 illustrates their LCCA result.

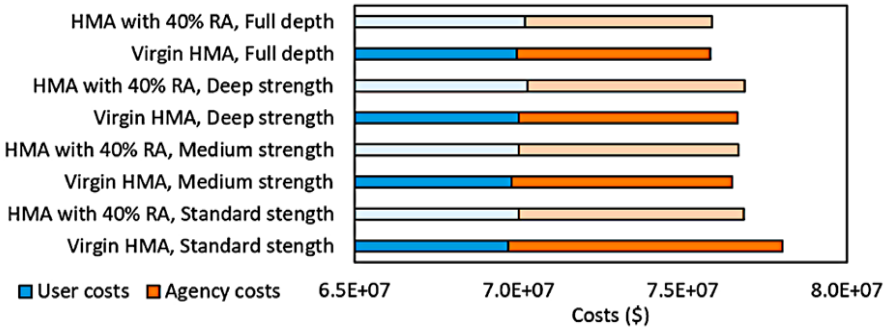

Figure 2.14. LCCA results for RAP usage in pavement construction. [Qiao et al. (2019)].

Chapter 3 Materials and Laboratory Tests

This chapter presents experimental efforts to characterize the linear viscoelastic and fracture properties of selected pavement mixtures subjected to various loading rates at different temperatures. To that end, two laboratory tests - uniaxial compressive cyclic tests to identify the linear viscoelastic properties and semi-circular bending (SCB) fracture tests to characterize the fracture properties of mixtures were conducted.

3.1 Material selection

Two different sources of RAP materials (i.e., poor quality and good quality) included in three mixes (i.e., SPR, SRM, and SLX) were considered in this research for mixture evaluation. Toward this end, NDOT engineers investigated construction projects, and the following two projects were selected to collect source materials.

- Good-quality RAP: Project: 15-4(120), Nebraska Highway 15
- Poor-quality RAP: Project: 23-2(128), Nebraska Highway 23

The collected materials include three asphalt mixes (SPR, SLX, and SRM) with consistent RAP materials (in two different qualities), so that laboratory tests of six mixes (i.e., three types of asphalt mixes with two different RAPs) can be used directly to compare properties and to obtain performance characteristics of pavement structures with different overlay configurations. The laboratory testing also included evaluation of the RAP quality by extracting and grading the binder and determining RAP aggregate consensus properties. Table 3.1 represent the binder properties for all the mixtures.

Table 3.1. Binder Properties

Mixtures	PG (C)		BBR					
	Low-End	High-End	-24 C		-18 C		-12 C	
			S-value	M-value	S-value	M-value	S-value	M-value
Good SLX-RAP	-	77.3	415	0.283	206	0.351	-	-
Good SRM-RAP	-	80.0	473	0.273	234	0.329	-	-
Good SPR-RAP	-	77.9	433	0.272	204	0.334	-	-
Bad SLX-RAP	-	75.4	371	0.264	182	0.308	-	-
Bad SRM-RAP	-	79.0	-	-	283	0.281	132	0.330
Bad SPR-RAP	-	81.0	-	-	282	0.282	139	0.317

3.2 Laboratory tests

Laboratory tests were performed to characterize mixture properties at two different temperature regimes, intermediate and low, because the primary pavement distresses studied in this research were two different types of cracking: thermal cracking which happens at low temperatures and reflective cracking, which is induced by truck loading and also associated with existing underlying thermal cracks. For the six mixes, two laboratory tests were performed: (1) dynamic modulus test to identify temperature–frequency-dependent stiffness characteristics of mixtures and (2) semi-circular bending fracture tests to obtain fracture properties of mixtures at an intermediate testing temperature (23°C) and a low temperature (–10°C). Figure 3.1 presents the testing station (UTM-25kN), and specimen geometries for two mechanical tests. The UTM-25kN is a computer-controlled hydraulic testing machine capable of subjecting a compacted asphalt mixture specimen to static or cyclic loading over a range of temperatures and frequencies.

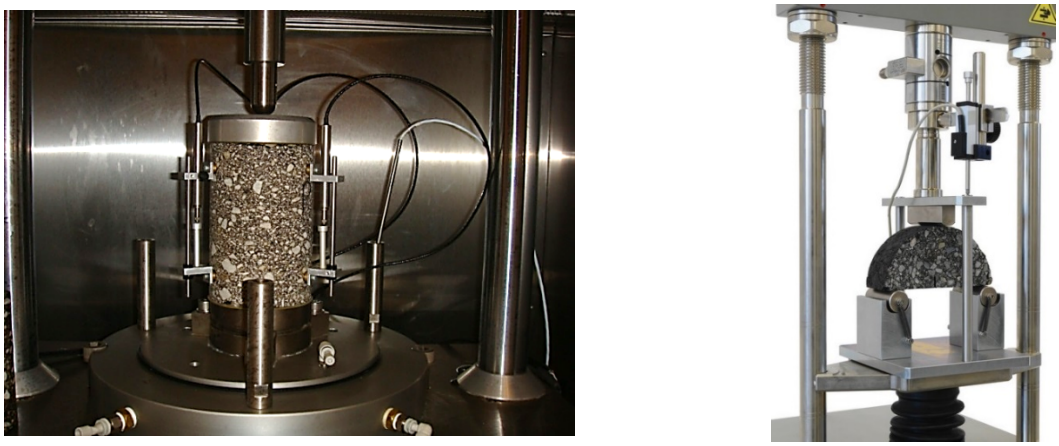

(a) (b)

Figure 3.1. Material testing machines: a) Uniaxial compressive cyclic test, and b) SCB Fracture test.

Figure 3.2 briefly illustrates the process of sample fabrication and laboratory tests performed for this study. As it was noted, laboratory tests were conducted to obtain linear viscoelastic properties and to characterize the fracture properties of the mixture. As shown, cylindrical mixture samples were fabricated using a Superpave gyratory compactor (SGC). Two different specimen geometries were extracted from the SGC samples. They were (1) cylindrical cores (150 mm in height and 100 mm in diameter) to be used for determining the linear viscoelastic properties of the mixture and (2) semi-circular bending (SCB) specimens (150 mm in diameter and 50-mm thick with a 2-mm-wide and 15 mm-deep mechanical notches) to be used for fracture tests of the mixture.

(a)

(b)

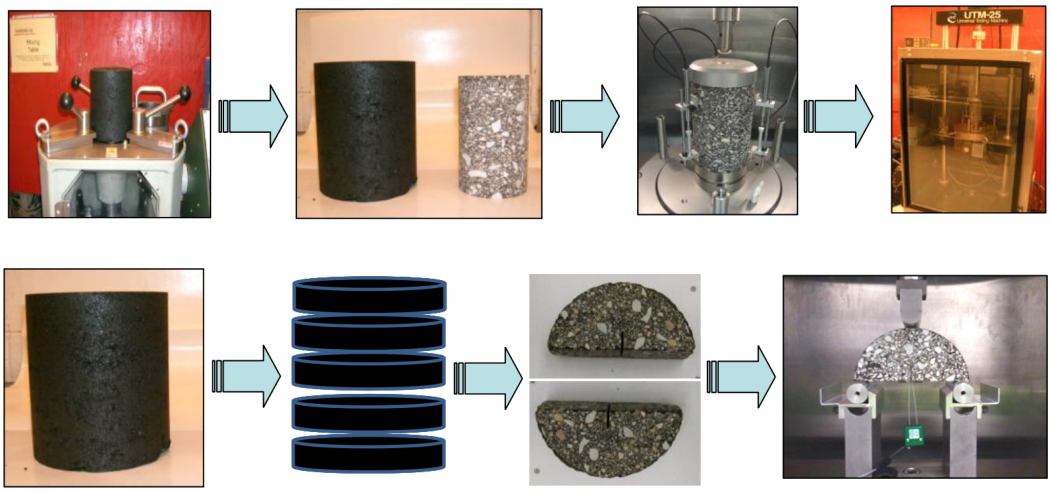

Figure 3.2. Specimen fabrication process for: a) LVE test, and b) SCB test.

3.2.1 Dynamic modulus tests for linear viscoelastic properties

Uniaxial compressive cyclic tests were performed for the linear viscoelastic stiffness of the mixtures. The loading levels were carefully adjusted until the strain levels were within the range of 0.000050 –0.000075. Three linear variable differential transformers (LVDTs) were mounted onto the surface of the specimen at 120° radial intervals with a 100 mm gauge length. As suggested in the AASHTO TP 62 (2008), five temperatures (-10, 4.4, 21.1, 37.8, and 54.4°C) and six loading frequencies (25, 10, 5, 1.0, 0.5, and 0.1 Hz) were used, and the frequency-temperature superposition concept was applied to obtain the linear viscoelastic master curves of the storage modulus in the frequency domain for a target reference temperature. The testing results of the storage modulus, as a function of angular frequency, were then fitted with a mathematical function (i.e., Prony series) based on the generalized Maxwell model as follows.

$$E'(\omega) = E_\infty + \sum_{i=1}^{n} \frac{E_i\,\omega^2\,{\rho_i}^2}{\omega^2\,{\rho_i}^2 + 1} \qquad (3.1)$$

where,

$E'(\omega)$ = storage modulus,

ω = angular frequency,

E_∞ = long-time equilibrium modulus,

E_i = spring constants in the generalized Maxwell model,

ρ_i = relaxation time, and

n = number of Maxwell units in the generalized Maxwell model.

Using the Prony series parameters E_∞, E_i, and ρ_i obtained by fitting the experimental data with a storage modulus, the relaxation modulus could be expressed in the time domain as follows:

$$E(t) = E_\infty + \sum_{i=1}^{n} E_i \, e^{-\frac{t}{\rho_i}} \tag{3.2}$$

where,

$E(t)$ = relaxation modulus in the time domain, and

t = loading time.

A total of three replicates were tested for each of six mixtures, and the values of the storage modulus at each different testing temperature, over the range of the loading frequencies, were obtained. Figure 3.3 presents the test results. The test results among the replicates at the same testing conditions were generally repeatable without large discrepancies.

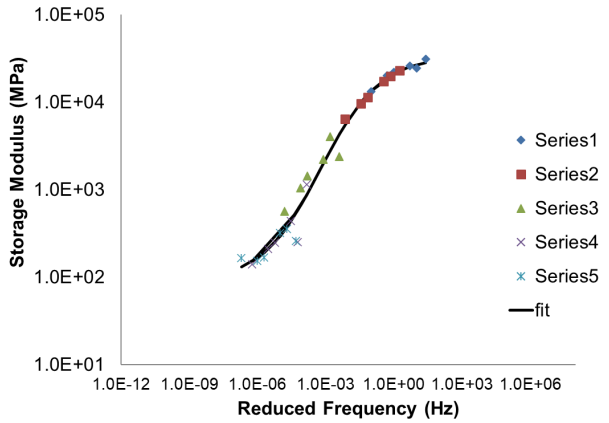

SLX with good RAP

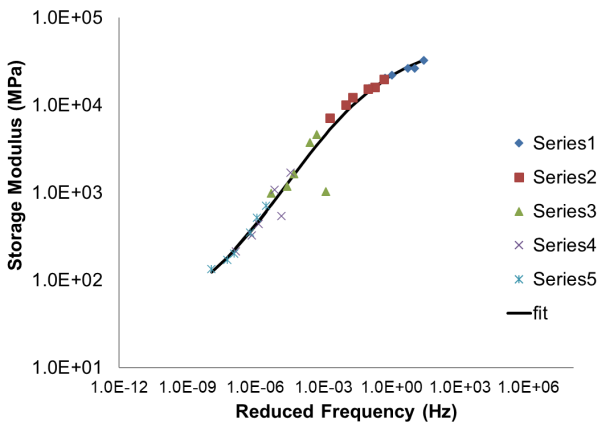

SLX with poor RAP

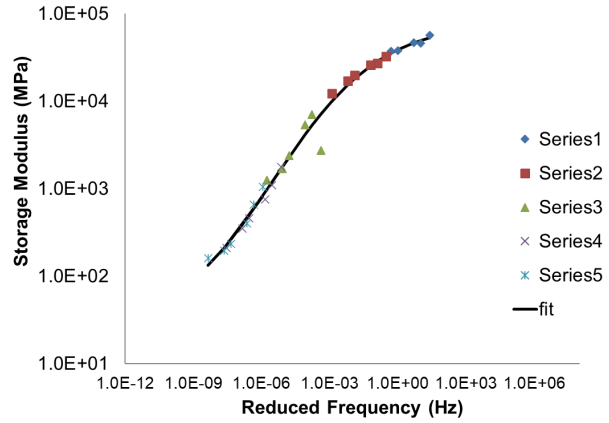

SPR with good RAP

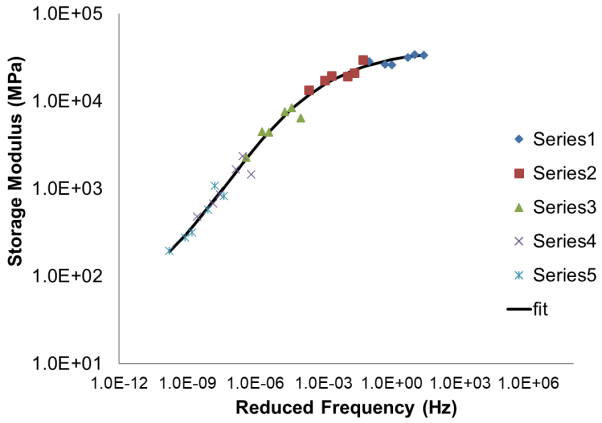

SPR with poor RAP

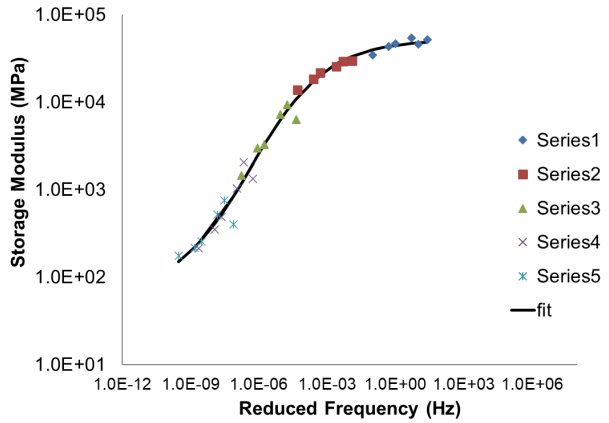

SRM with good RAP

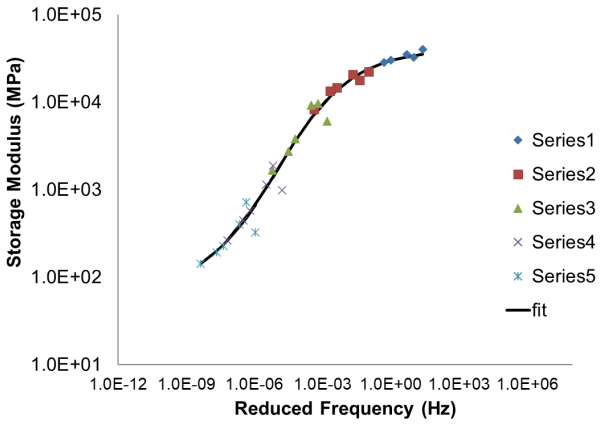

SRM with poor RAP

Figure 3.3 Dynamic modulus test results.

The test results from replicates were then averaged to produce 30 individual storage moduli at all levels of temperature and frequency, to produce a stiffness master curve constructed at a reference temperature. The master curve represents the stiffness of the mixture in a wide range of loading frequencies (or loading times, equivalently). Master curves were constructed using the time (or frequency) - temperature superposition by shifting data at various temperatures, with respect to loading frequency, until the curves merged into a single smooth function. After the shifting was completed, the master curve, at an arbitrary reference temperature, was then fitted with the Prony series (Eq. 3.2) to determine linear viscoelastic material parameters.

The difference in the materials' viscoelastic stiffness at two different quality levels is shown in Figure 3.4. These material properties are related to their behavior at intermediate temperature (i.e. 23 ºC). As can be seen, for good-quality materials, the viscoelastic stiffness of SLX mix is lower than the other mixes. It is expected since the RAP content in SPR and SRM is higher, leading them to be stiffer. For poor-quality materials, the SLX and SRM show less stiffness and SPR gets higher values. At earlier stages SLX shows more compliance and its stiffness gets closer to the poor SRM as time goes on. This comes from the environmental related conditions that mixes experienced. This high level of stiffness for poor quality SPR makes issues when repetitive mechanical loads are considered. Considering its less compliance, poor quality SPR is highly expected to cease resisting to fatigue cracking.

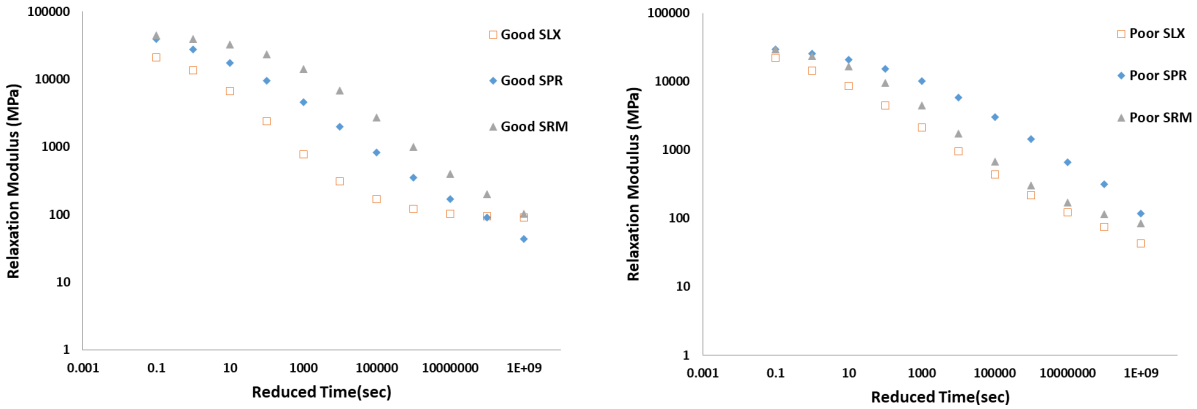

(a) (b)

Figure 3.4. Difference in stiffness at intermediate temperature for: a) good-, and b) poor-quality mixes.

At low temperature (-10 ºC), the asphalt mixes show almost similar relaxation modulus, yet the SLX has slightly lower stiffness because of lower RAP content in it, as shown in Figure 3.5.

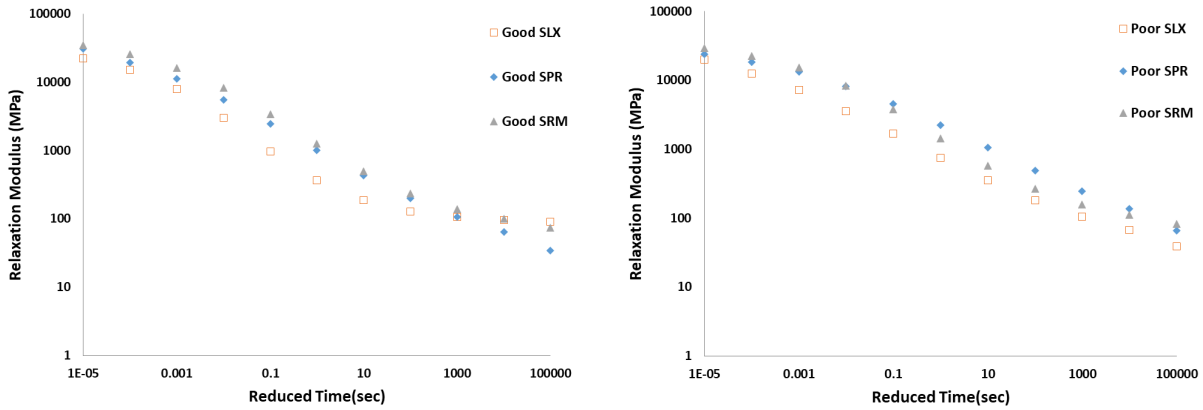

(a) (b)

Figure 3.5. Difference in stiffness at low temperature for: a) good-, and b) poor-quality mixes.

Table 3.2, 3.3, and 3.4 present the Prony series parameters determined for each mixture at different reference temperatures. Among them, the Prony series parameters at the reference temperature of -10ºC were used for the low temperature-pavement performance simulation in Chapter 4.

Table 3.2. Prony series parameters for SLX mix at different reference temperatures

Material	Good-quality SLX				Poor-quality SLX			
Ref. Temp.	-10		23		-10		23	
Prony Series Parameter	E_i (MPa)	ρ_i (sec)	E_i (MPa)	ρ_i (sec)	E_i (MPa)	ρ_i (sec)	E_i (MPa)	ρ_i (sec)
1	2.12E+04	1.00E-01	2.25E+04	1.00E-05	2.24E+04	1.00E-01	2.00E+04	1.00E-05
2	1.36E+04	1.00E+00	1.52E+04	1.00E-04	1.45E+04	1.00E+00	1.24E+04	1.00E-04
3	6.73E+03	1.00E+01	7.98E+03	1.00E-03	8.69E+03	1.00E+01	7.20E+03	1.00E-03
4	2.41E+03	1.00E+02	3.03E+03	1.00E-02	4.48E+03	1.00E+02	3.58E+03	1.00E-02
5	7.85E+02	1.00E+03	9.78E+02	1.00E-01	2.14E+03	1.00E+03	1.67E+03	1.00E-01
6	3.10E+02	1.00E+04	3.65E+02	1.00E+00	9.56E+02	1.00E+04	7.45E+02	1.00E+00
7	1.72E+02	1.00E+05	1.89E+02	1.00E+01	4.42E+02	1.00E+05	3.52E+02	1.00E+01
8	1.23E+02	1.00E+06	1.29E+02	1.00E+02	2.18E+02	1.00E+06	1.79E+02	1.00E+02
9	1.04E+02	1.00E+07	1.07E+02	1.00E+03	1.22E+02	1.00E+07	1.05E+02	1.00E+03
10	9.57E+01	1.00E+08	9.68E+01	1.00E+04	7.58E+01	1.00E+08	6.72E+01	1.00E+04
11	9.11E+01	1.00E+09	9.13E+01	1.00E+05	4.28E+01	1.00E+09	3.90E+01	1.00E+05
Inf.	89.31	-	89.22	-	28.25	-	25.97	-

Table 3.3. Prony series parameters for SPR mix at different reference temperatures

Material	Good-quality SPR				Poor-quality SPR			
Ref. Temp.	-10		23		-10		23	
Prony Series Parameter	E_i (MPa)	ρ_i (sec)	E_i (MPa)	ρ_i (sec)	E_i (MPa)	ρ_i (sec)	E_i (MPa)	ρ_i (sec)
1	3.94E+04	1.00E-01	3.08E+04	1.00E-05	3.00E+04	1.00E-01	2.40E+04	1.00E-05
2	2.76E+04	1.00E+00	1.95E+04	1.00E-04	2.57E+04	1.00E+00	1.85E+04	1.00E-04
3	1.76E+04	1.00E+01	1.13E+04	1.00E-03	2.09E+04	1.00E+01	1.32E+04	1.00E-03
4	9.60E+03	1.00E+02	5.49E+03	1.00E-02	1.54E+04	1.00E+02	8.24E+03	1.00E-02
5	4.63E+03	1.00E+03	2.44E+03	1.00E-01	1.02E+04	1.00E+03	4.56E+03	1.00E-01
6	1.99E+03	1.00E+04	1.00E+03	1.00E+00	5.91E+03	1.00E+04	2.25E+03	1.00E+00
7	8.28E+02	1.00E+05	4.31E+02	1.00E+01	3.05E+03	1.00E+05	1.05E+03	1.00E+01
8	3.56E+02	1.00E+06	1.99E+02	1.00E+02	1.44E+03	1.00E+06	4.89E+02	1.00E+02
9	1.71E+02	1.00E+07	1.07E+02	1.00E+03	6.67E+02	1.00E+07	2.47E+02	1.00E+03
10	9.19E+01	1.00E+08	6.39E+01	1.00E+04	3.17E+02	1.00E+08	1.38E+02	1.00E+04
11	4.40E+01	1.00E+09	3.46E+01	1.00E+05	1.19E+02	1.00E+09	6.58E+01	1.00E+05
Inf.	24.18	-	21.62	-	42.86	-	35.3	-

Table 3.4. Prony series parameters for SRM mix at different reference temperatures

Material	Good-quality SRM				Poor-quality SRM			
Ref. Temp.	-10		23		-10		23	
Prony Series Parameter	E_i (MPa)	ρ_i (sec)	E_i (MPa)	ρ_i (sec)	E_i (MPa)	ρ_i (sec)	E_i (MPa)	ρ_i (sec)
1	4.47E+04	1.00E-01	3.47E+04	1.00E-05	3.00E+04	1.00E-01	2.90E+04	1.00E-05
2	3.97E+04	1.00E+00	2.57E+04	1.00E-04	2.40E+04	1.00E+00	2.25E+04	1.00E-04
3	3.26E+04	1.00E+01	1.63E+04	1.00E-03	1.68E+04	1.00E+01	1.53E+04	1.00E-03
4	2.35E+04	1.00E+02	8.30E+03	1.00E-02	9.67E+03	1.00E+02	8.39E+03	1.00E-02
5	1.42E+04	1.00E+03	3.44E+03	1.00E-01	4.49E+03	1.00E+03	3.74E+03	1.00E-01
6	6.84E+03	1.00E+04	1.26E+03	1.00E+00	1.76E+03	1.00E+04	1.44E+03	1.00E+00
7	2.71E+03	1.00E+05	4.95E+02	1.00E+01	6.84E+02	1.00E+05	5.70E+02	1.00E+01
8	9.95E+02	1.00E+06	2.34E+02	1.00E+02	3.06E+02	1.00E+06	2.67E+02	1.00E+02
9	4.04E+02	1.00E+07	1.40E+02	1.00E+03	1.72E+02	1.00E+07	1.57E+02	1.00E+03
10	1.99E+02	1.00E+08	9.95E+01	1.00E+04	1.17E+02	1.00E+08	1.11E+02	1.00E+04
11	1.02E+02	1.00E+09	7.47E+01	1.00E+05	8.47E+01	1.00E+09	8.24E+01	1.00E+05
Inf.	66.72	-	64.34	-	71.72	-	70.88	-

3.2.2 SCB tests for fracture properties

To characterize the fracture properties of asphalt mixtures, researchers in the asphaltic materials and pavement mechanics field have typically pursued four geometries, which are listed and referenced in Table 3.5.

Table 3.5. Fracture tests reviewed in the literature

Specimen Geometries	Research
single-edge notched beam, SE(B)	• Mobasher et al. 1997 • Hoare and Hesp 2000 • Marasteanu et al. 2007
disc-shaped compact tension, DC(T)	• Lee et al. 1995 • Wagoner et al. 2005 • Wagoner et al. 2006
semi-circular bending, SCB	• Molenaar et al. 2002 • Li and Marasteanu 2004 • van Rooijen and de Bondt 2008 • Li and Marasteanu 2010 • Aragao 2011
double-edged notched tension, DENT	• Seo et al. 2002

Among the various options, SCB testing was selected in this study because it has several benefits compared to other fracture test methods. Even if it has some limitations (Wagoner et al. 2005), SCB testing is particularly attractive in that it is repeatable, simple to perform, and that multiple testing specimens can easily be prepared through a routine process of mixing and Superpave gyratory compacting of asphalt mixtures. Furthermore, the SCB geometry is even more attractive considering the fracture characteristics of field cores, which are usually circular. Based on these practical benefits, the SCB testing configuration has become a popular geometry for evaluating the fracture behavior of bituminous mixtures. Before testing, individual SCB specimens were placed inside the environmental chamber of a mechanical testing machine for temperature equilibrium targeting the two different testing temperatures (low: -10°C and intermediate: 23°C). Following the temperature conditioning step, specimens were subjected to a simple three-point bending configuration with a monotonic displacement rate of 3 mm/min applied to the top centerline of the SCB specimens at each testing temperature. Metallic rollers, separated by 120 mm (15 mm from the edges of the specimen at each end), were used to support the specimen. Reaction force at the loading point and vertical crosshead displacements were monitored by the data acquisition system installed on the mechanical testing machine. A total of 36 SCB specimens

were prepared to complete three replicates per test case of the twelve test cases in total (six mixtures at two different temperatures). In an attempt to illustrate the effects of testing conditions on the mixtures fracture behavior, Figure 3.6 presents the SCB test results by plotting the average values between the reaction forces and loading point displacements for different mixtures and temperatures.

It can be inferred from the results that the quality of mixes is directly related to their fracture behavior. Mixtures made with poor-quality RAP show steeper slope in both elastic and post peak regimes compared to the mixes with good-quality RAP. Moreover, the effect of temperature on the fracture behavior of mixes is noticeable. There is a sharp increase in load-displacement curves at -10C. The peak force decreases as the temperature elevates. Therefore, it appears that the fracture behavior is severely temperature-dependent, which is typically observed from a linear elastic fracture state. The trends presented in Figure 3.6 and 3.7 suggest that the temperature-dependent nature of the fracture characteristics needs to be considered when modeling the mechanical performance of asphalt mixtures and pavements with different service temperatures.

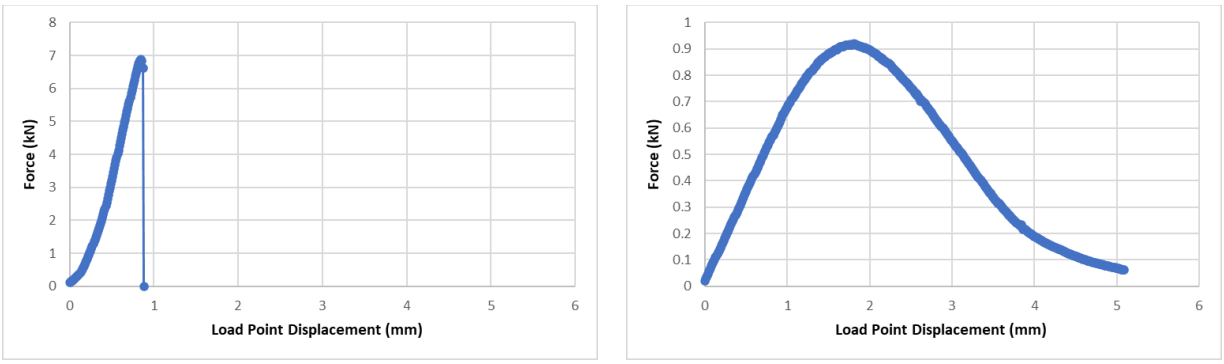

(a)

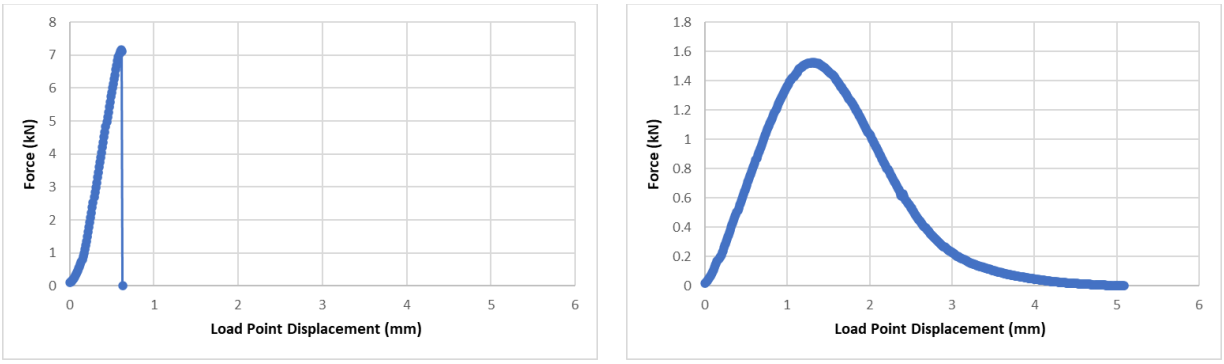

(b)

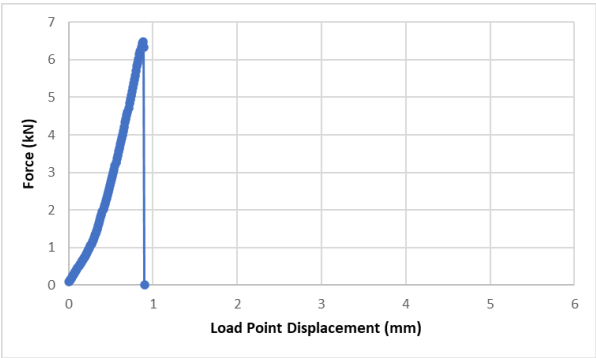
Force (kN)
Load Point Displacement (mm)

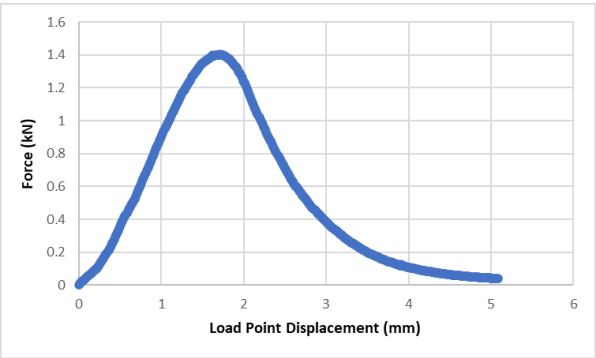
Force (kN)
Load Point Displacement (mm)

(c)

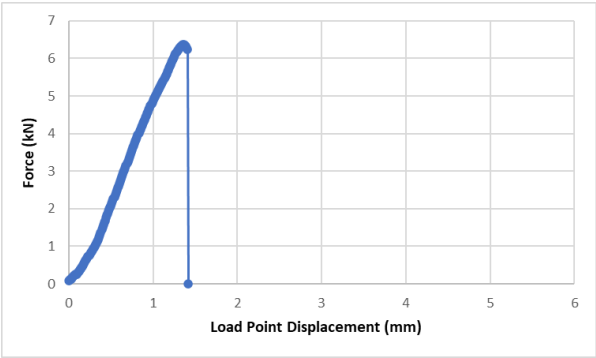
Force (kN)
Load Point Displacement (mm)

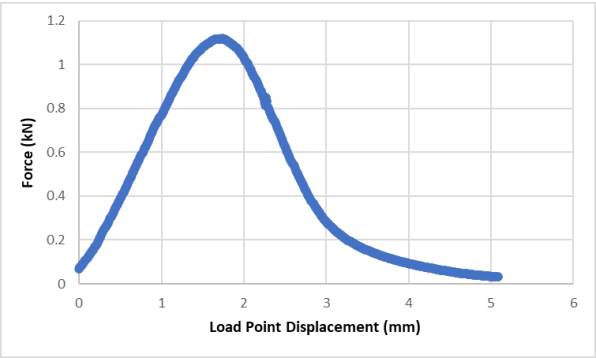
Force (kN)
Load Point Displacement (mm)

(d)

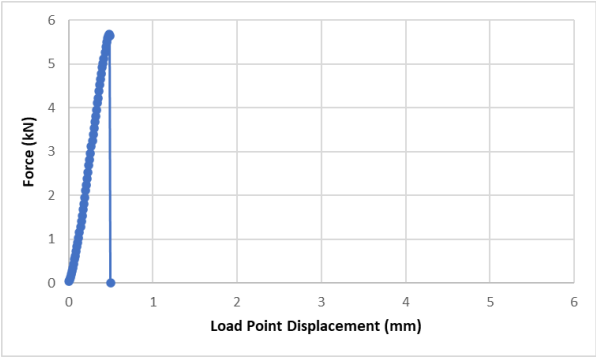
Force (kN)
Load Point Displacement (mm)

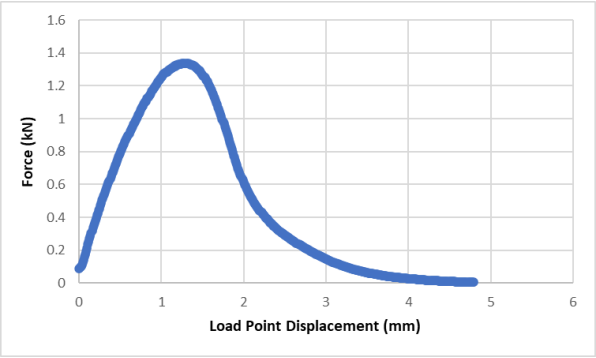
Force (kN)
Load Point Displacement (mm)

(e)

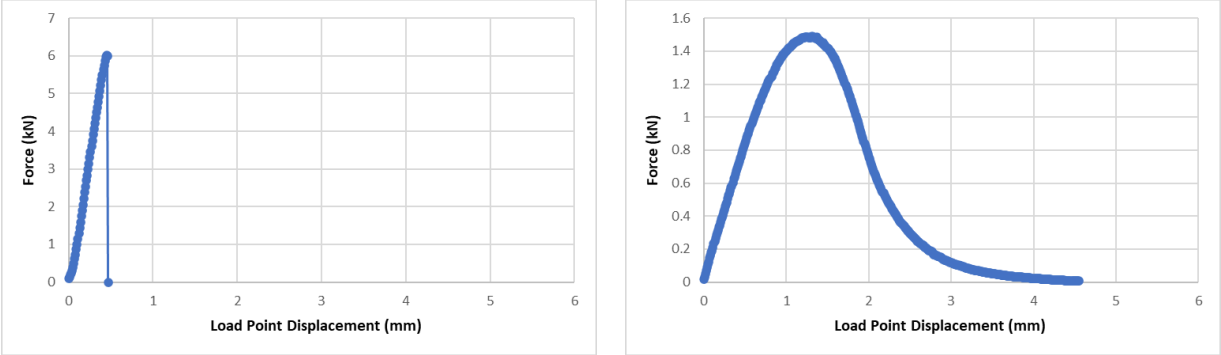

(f)

Figure 3.6. SCB fracture test result at low temperature (left) and intermediate temperature (right) for: a) good-quality SLX, b) good-quality SPR, c) good-quality SRM, d) poor-quality SLX, e) poor-quality SPR, and f) poor-quality SRM.

The fracture properties of mixes at two material quality level and two temperature are compared as shown in Figure 3.7. As it can be seen in the Figure 3.7, the SLX mixtures at both quality levels are more compliant at intermediate temperature. This will lead to good cracking performance for mechanical induced reflective cracking, and fatigue cracking. The initial slope of the curves clearly demonstrates that the poor-quality materials show higher stiffness. This stiffness should be further used in fracture mechanics approach to govern the behavior of the cracking process. Hence, with a specific displacement in material domain, higher risk of cracking is expected for those cases with higher stiffness. It should be noted that the low temperature for testing two mixes, good-quality SRM and poor-quality SLX, was -2C, while for the rest of the cases, the low temperature SCB test was set to -10C.

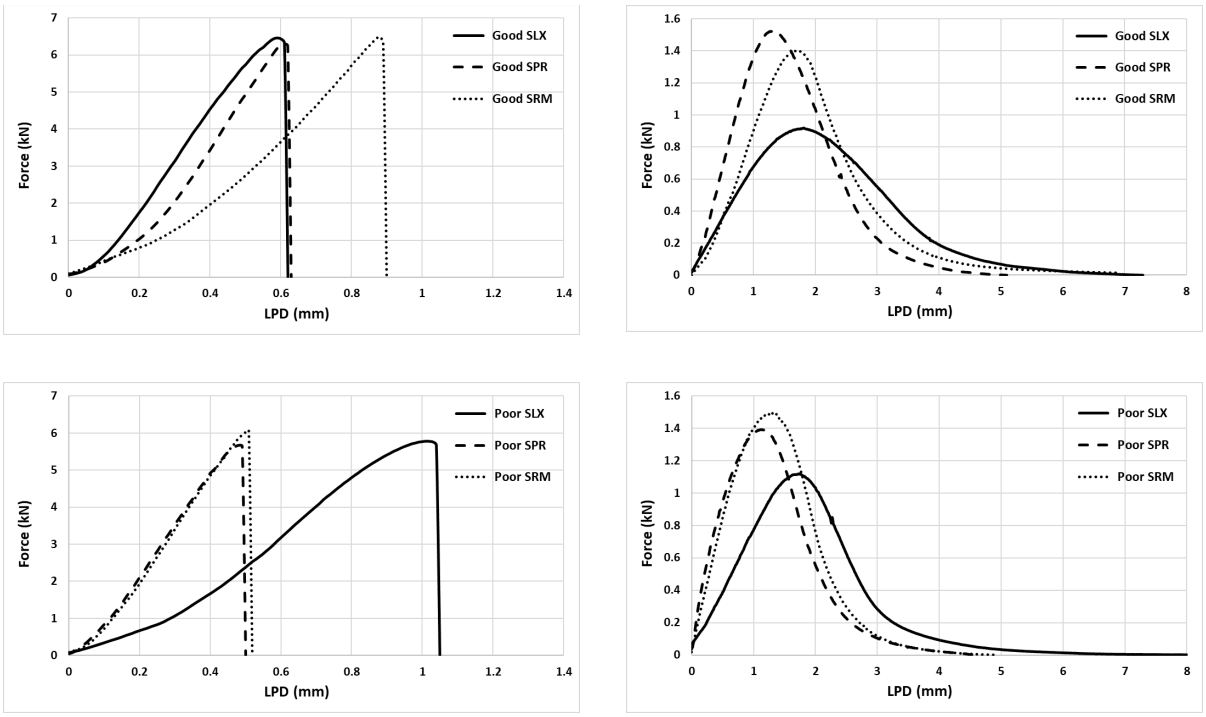

Figure 3.7. comparison of SCB fracture test results at low temperature (left) and intermediate temperature (right).

Figure 3.8 presents visual observation of SCB specimens after testing at the two different temperatures. The cracking pattern is presented in Figure 3.8(a), and the fracture surfaces of individual specimens are shown in Figure 3.8(b). It appears that cracks propagated straight from the crack tip and travelled through the aggregates. Therefore, mode-I cracking should be sufficient when considering computational modeling.

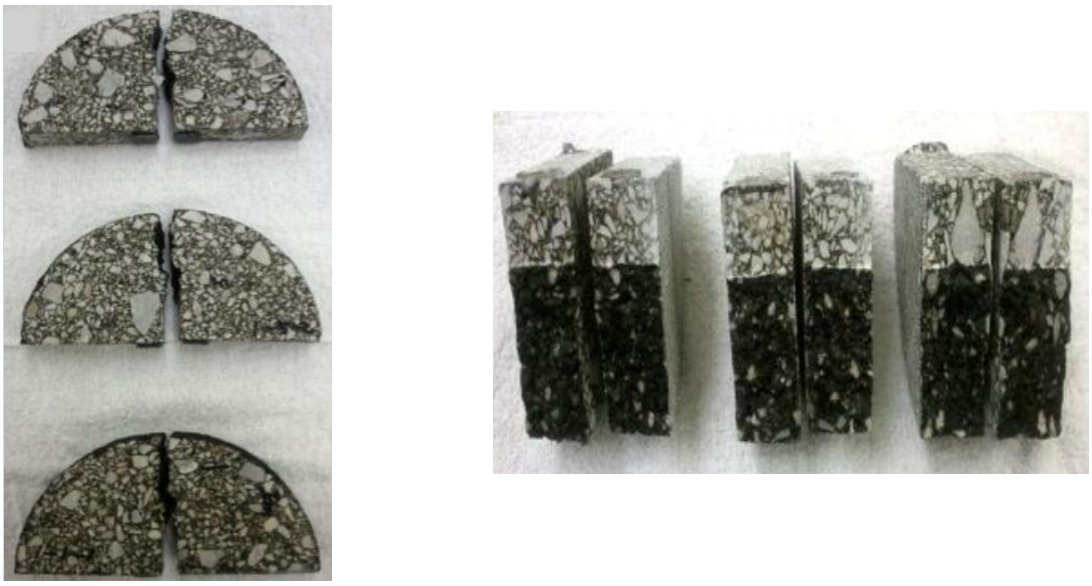

(a) (b)

Figure 3.8. Visual observation of SCB specimens at low temperature after testing: a) cracking pattern and b) fractured surface.

Chapter 4 Modeling and Simulation Results

In this chapter, a mechanistic approach was used to simulate pavement response to thermal-mechanical loads through finite element method (FEM). To do so, initially, the parameters of the damage model used in FEM to simulate fracture were calibrated. Then, one of the most common asphaltic pavement structures in Nebraska (with 4-inch overly) was modeled using a two-dimensional FEM to investigate the overall performance of the pavement subjected to thermal (low temperature) and mechanical loadings. The 2-D finite element modeling was carried out using a well-known commercial package, ABAQUS version 6.14 (2014), with the mechanical material properties as obtained from the experiments presented in Chapter 3. The FEM simulation also employed a user-defined temperature subroutine, UTEMP, to represent the temporal and spatial temperature profile effectively in the pavement structure. The reflective cracking due to temperature variation and mechanical loading in the asphalt overlay layer was simulated for parametric analyses by varying overlay configuration and material properties. The expected results could lead to helping pavement engineers understand the sensitivity of rehabilitation practices on the RAP material they are using and the overall responses and performance characteristics of pavement structures. Consequently, it can enable engineers to select materials for rehabilitation practices in a more appropriate way.

4.1 Governing equations for FEM

In this study, a thermo-viscoelastic model with cohesive zone fracture was employed for simulating the fracture behavior of the asphalt layer when the pavement was subjected to varying low temperatures and mechanical truck loading. In order to avoid unnecessary complexities at this stage, the inertial effects of the dynamic traffic loads, body forces, and large deformations were ignored so that the problem could be simplified to quasi-static small strain conditions.

It is crucial to select appropriate constitutive models for bulk materials in finite element modeling. For the modeling of old asphalt layer and subgrade, linear thermo-elastic behavior was considered. The linear thermo-elastic constitutive equation can be written as follows

$$\sigma_{ij}(x_m, t) = C_{ijkl}(x_m)\left\{\varepsilon_{kl}(x_m, t) - \varepsilon_{kl}^{\theta}(x_m, t)\right\} \quad (4.1)$$

$$\varepsilon_{kl}^{\theta}(x_m, t) = \alpha_{kl}(x_m)\{\theta(x_m, t) - \theta^{R}(x_m, t)\} \quad (4.2)$$

where,

σ_{ij} = stress tensor,

ε_{kl} = strain tensor,

C_{ijkl} (x_m) = elastic modulus tensor,

α_{kl} = coefficient of thermal expansion,

θ (x_m,t) = temperature at a particular position and at a specific time,

θ^R (x_m) = stress-free reference temperature, and

x_m = spatial coordinates.

Asphalt concrete material placed on top of the existing old asphalt layer was modeled as linear, thermo-rheologically simple, and non-aging viscoelastic, with its constitutive equation expressed as follows:

$$\sigma_{ij}(x_m,t) = \int_0^{\xi} C_{ijkl}\,(x_m,\xi-\tau)\frac{\partial \varepsilon_{kl}(x_m,\tau)}{\partial \tau}d\tau - \int_0^{\xi} \beta_{ij}\,(x_m,\xi-\tau)\frac{\partial \theta(x_m,\tau)}{\partial \tau}d\tau \qquad (4.3)$$

$$\beta_{ij}\,(x_m,\xi) = C_{ijkl}\,(x_m,\xi)\,\alpha_{kl}(x_m) \qquad (4.4)$$

where,

C_{ijkl} (x_m,ξ) = thermo-viscoelastic relaxation modulus tensor,

β_{ij} (x_m,ξ) = second-order tensor of relaxation modulus relating stress to temperature variations,

ξ = reduced time, and

τ = time integration variable.

The reduced time can be defined as follows:

$$\xi(t) = \int_0^t \frac{1}{a_T(\theta(t))} \qquad (4.5)$$

where,

t = real time, and

a_T = temperature shift factor.

The temperature shift factor, $a_T(\theta(t))$, is generally described by either the Arrhenius or the WLF equations (Williams et al. 1955). In the present study, the shift factor was described according to the WLF equation:

$$\log_{10}(a_T) = \frac{-C_1(\theta - \theta^R)}{C_2 + (\theta - \theta^R)} \tag{4.6}$$

where,

C_1 and C_2 = model constants.

The thermo-viscoelastic relaxation modulus of asphalt concrete was determined by performing laboratory tests, such as dynamic frequency sweep tests, within the theory of linear viscoelasticity, and test results were mathematically expressed in the form of a Prony series, as described comprehensively in Chapter 3. Also, the cohesive zone model was used to simulate the fracture process of asphalt surface layers due to thermal-mechanical loading.

The fracture process zone (FPZ) is a nonlinear zone characterized by progressive softening, for which the stress decreases at increasing deformation. The nonlinear softening zone is surrounded by a non-softening nonlinear zone, which represents material inelasticity. Bazant and Planas (1998) skillfully classified the fracture process behavior in certain materials into three types: brittle, ductile, and quasi-brittle. Each type presents different relative sizes of those two nonlinear zones (i.e., softening, and non-softening nonlinear zones). Figure 4.1 presents the third type of behavior, the so-called quasi-brittle fracture. It includes situations in which a major part of the nonlinear zone undergoes progressive damage with material softening due to microcracking, void formation, interface breakages, frictional slips, and others forms of damage. The softening zone is then surrounded by the inelastic material-yielding zone, which is much smaller than the softening zone. This behavior includes a relatively large FPZ, as shown in the figure. Asphaltic paving mixtures are usually classified as quasi-brittle materials (Bazant and Planas 1998; Duan et al. 2006; Kim et al. 2008).

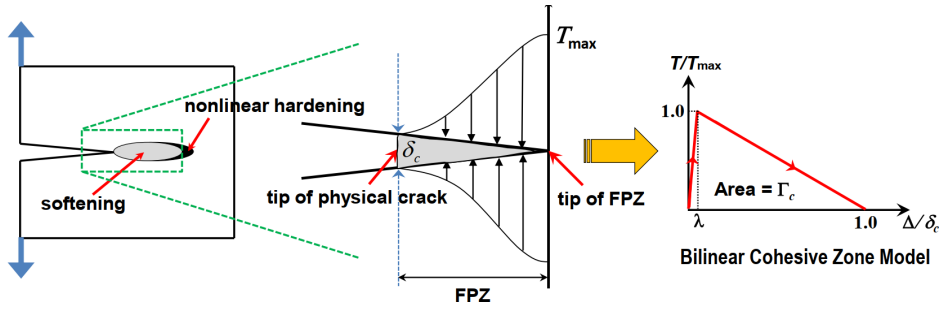

Figure 4.1 Schematic illustration of FPZ of typical quasi-brittle materials.

Cohesive zone models regard fracture as a gradual phenomenon in which separation (Δ) takes place across an extended crack tip (or cohesive zone) and where fracture is resisted by cohesive tractions (T). The cohesive zone effectively describes the material resistance when material elements are being displaced. Equations relating normal and tangential displacement jumps across the cohesive surfaces with the proper tractions define a cohesive zone model. Among numerous cohesive zone models developed for different specific purposes, this study used an intrinsic bilinear cohesive zone model (Geubelle and Baylor 1998; Espinosa and Zavattieri 2003; Song et al. 2006). As shown in figure 4.1, the model assumes that there is a recoverable linear elastic behavior until the traction (T) reaches a peak value, or cohesive strength (T_{max}), at a corresponding separation in the traction-separation curve. At that point, a non-dimensional displacement (λ) can be identified and used to adjust the initial slope in the recoverable linear elastic part of the cohesive law. This capability of the bilinear model to adjust the initial slope is significant because it can alleviate the artificial compliance inherent to intrinsic cohesive zone models. The λ value was determined through a convergence study designed to find a sufficiently small value to guarantee a level of initial stiffness that renders insignificant artificial compliance of the cohesive zone model. It was observed that a numerical convergence could be met when the effective displacement is smaller than 0.0005, which has been used for simulations in this study. Upon damage initiation, T varies from T_{max} to 0, when a critical displacement (δ_c) is reached and the faces of the cohesive element are separated fully and irreversibly. The cohesive zone fracture energy (Γ_c), which is the locally estimated fracture toughness, can then be calculated by computing the area below the bilinear traction-separation curve with peak traction (T_{max}) and critical displacement (δ_c) as follows:

$$\Gamma_c = \frac{1}{2}\delta_c T_{max} \tag{4.7}$$

4.2 Calibration of damage model parameters

To use SCB test results as the input for mathematical models, one should calibrate the model using the test data. First, the average fracture energy should be obtained for each test case. There are several methods (Wagoner et al. 2005; Marasteanu et al. 2007; Song et al. 2008; Aragao 2011) found in the literature to calculate the fracture energy. Among them, the finite element simulations of the SCB tests, with the cohesive zone model, were conducted to determine the fracture properties that are locally associated with initiating and propagating cracks through the specimens. Figure 4.2 presents a finite element mesh, which was finally chosen after conducting a mesh convergence study. The specimen was discretized using two-dimensional, three-node triangular elements for the bulk specimen, and zero-thickness cohesive zone elements were inserted along the center of the mesh to permit mode I crack growth in the simulation of SCB testing. The Prony series parameters (shown in table 3.2, 3.3, and 3.4), determined from the uniaxial compressive cyclic tests, were used for the viscoelastic elements, and the bilinear cohesive zone model illustrated in figure 4.1 was used to simulate fracture in the middle of the SCB specimen as the opening displacements increased.

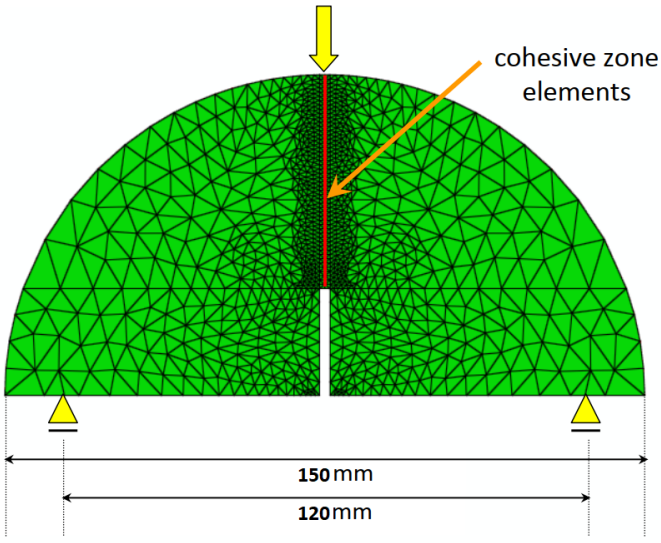

Figure 4.2. Finite element model mesh for SCB test.

The cohesive zone fracture properties (two independent values of the three: T_{max}, δ_c, and Γ_c) in the bilinear model were determined for each case through the calibration process until a good match between test results and numerical simulations was observed. Figure 4.3 presents a strong agreement between the test results (average of the three SCB specimens) and finite element simulations. As it was noted earlier, the SCB test temperature for poor-quality SLX and good-quality SRM was -2C while for the other mixtures it was -10C.

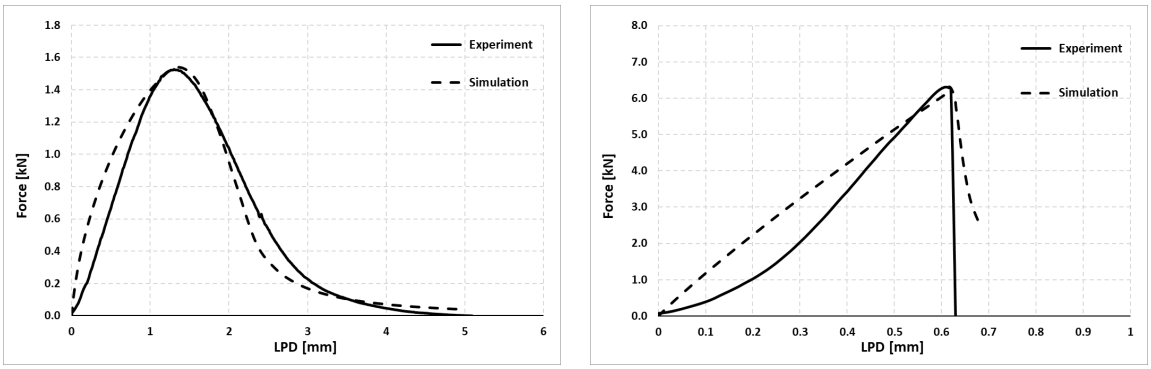

(a)

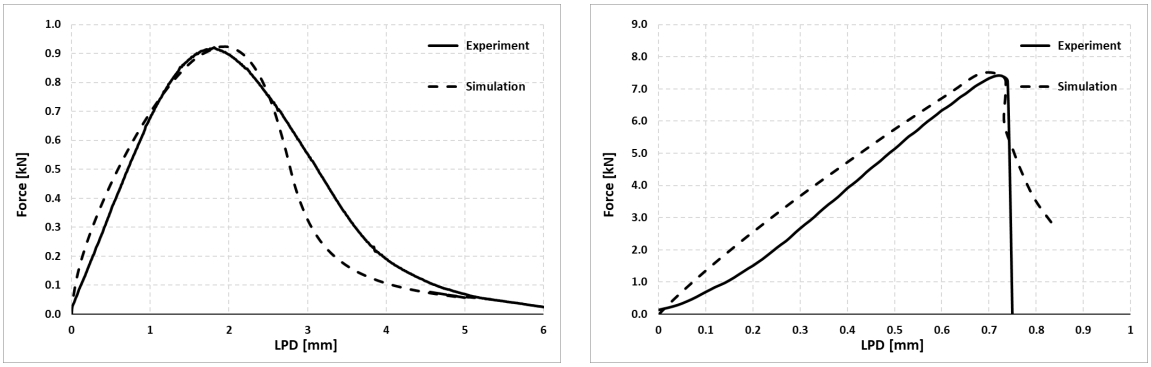

(b)

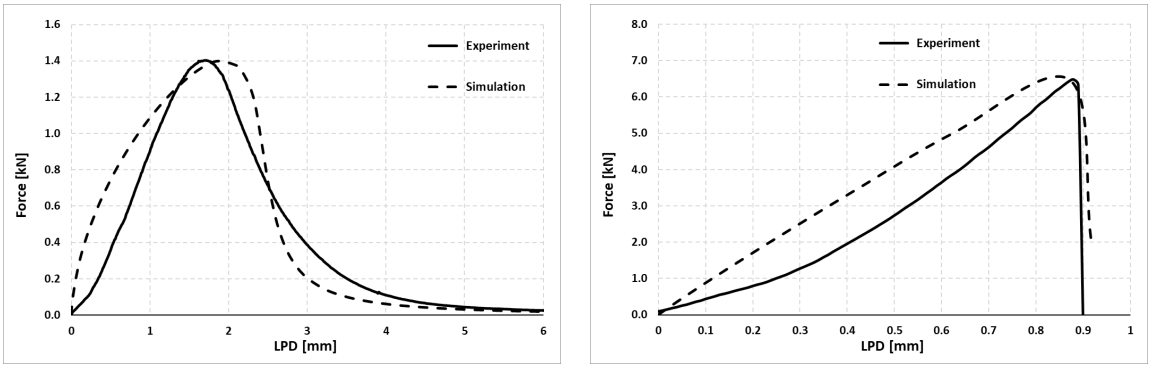

(c)

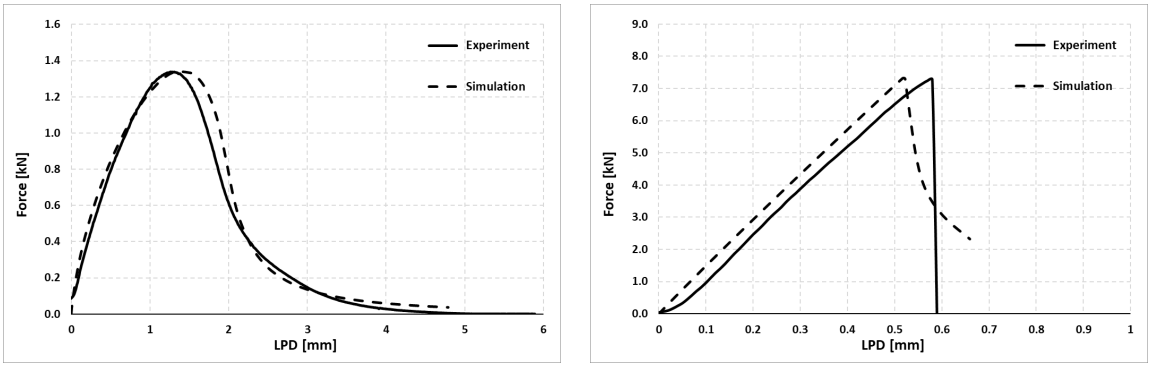

(d)

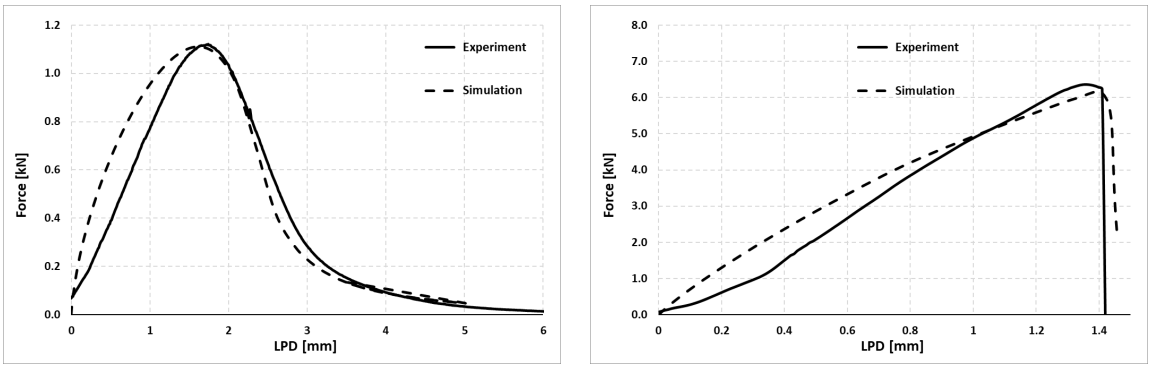

(e)

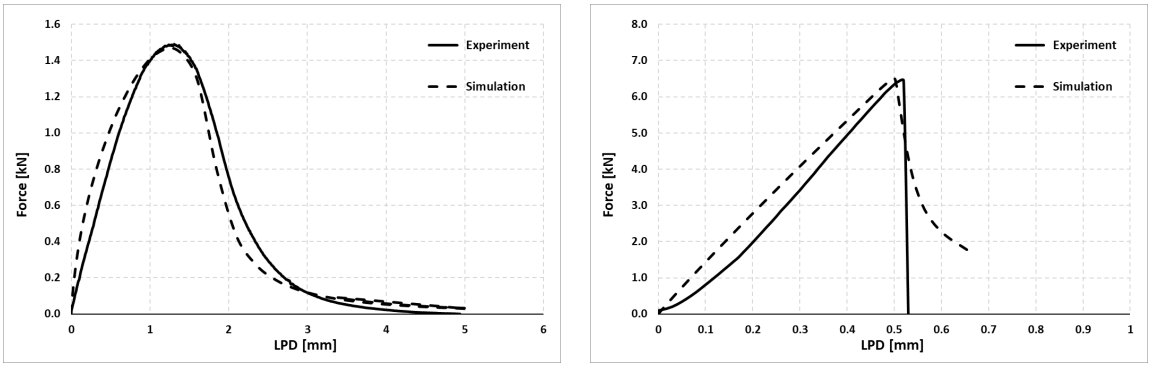

(f)

Figure 4.3. Calibration results at low temperature (right) and intermediate temperature (left) for: a) good SPR, b) good SLX, c) good SRM, d) poor SPR, e) poor SLX, and f) poor SRM.

Resulting calibrated fracture properties (T_{max} and Γ_c) at each testing temperature are presented in Table 4.1. Figure 4.4 shows the progressive damage evolution in SCB simulation.

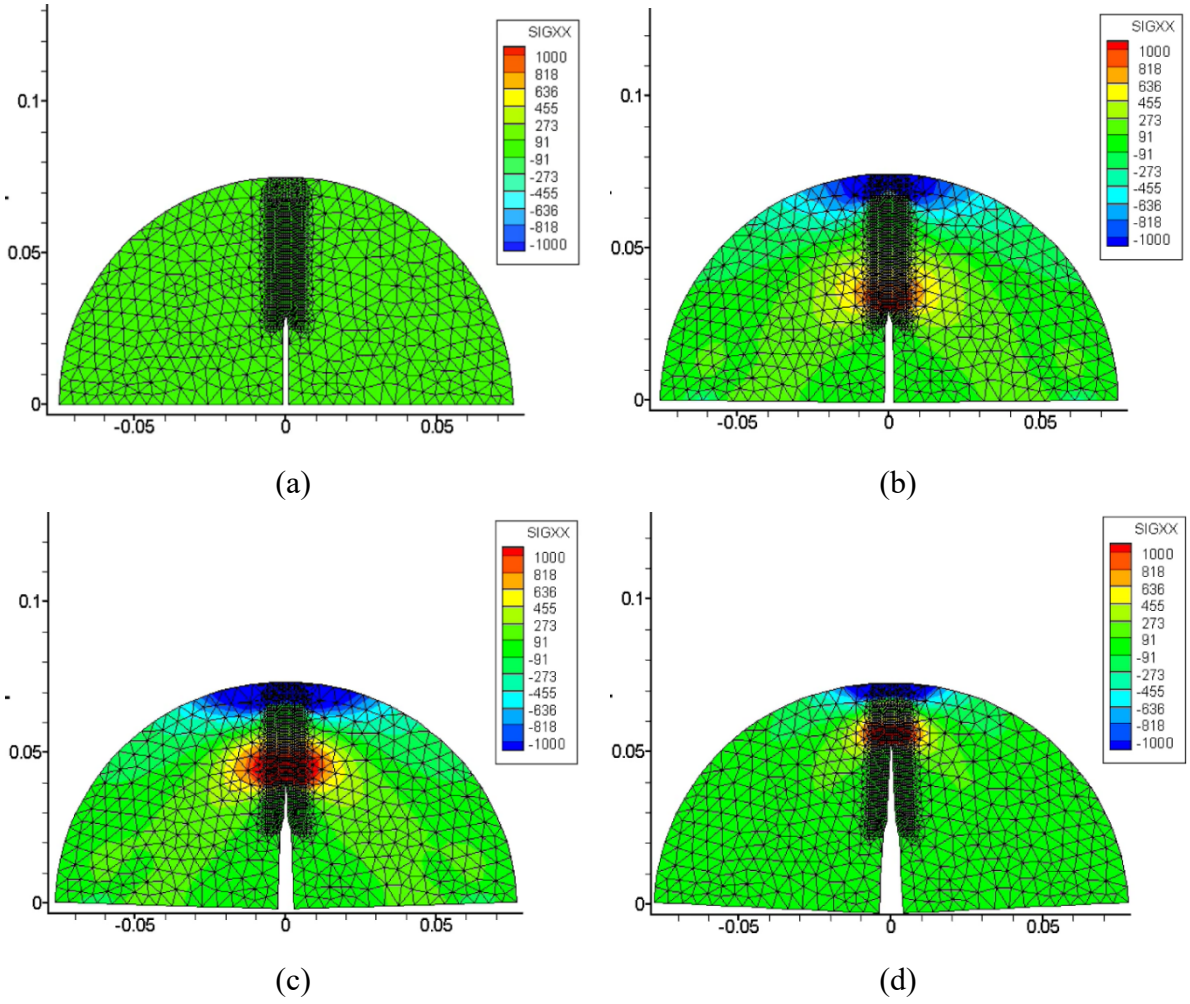

Figure 4.4. Contour plots of SCB test. Progressive damage evolution.

The agreement between tests and model simulations indicates that the local fracture properties were properly defined through the integrated experimental-numerical approach.

Table 4.1. Fracture properties of mixtures used in FEM

Material		Cohesive Zone Fracture Parameters at -10C		Cohesive Zone Fracture Parameters at 23C	
		T_{max} (kPa)	Γ_c (J/m^2)	T_{max} (kPa)	Γ_c (J/m^2)
SLX	Good	3650	350	210	310
	Poor	3550	250	255	310
SPR	Good	3100	220	380	335
	Poor	3450	220	325	290
SRM	Good	3000	250	370	270
	Poor	4000	200	355	290

4.3 Pavement geometry and boundary conditions

4.3.1 Pavement geometry

Figure 4.5 illustrates one of the common pavement configurations in Nebraska. As can be seen, there are three main sections in designing this pavement. In this configuration, 101.6 mm (4-inch) new asphalt overlay is laying on 177.8 mm of old asphaltic base and 152.4 mm of subgrade, which is soil. A length of 6 meters of the pavement profile was selected and considered in the finite element models due to repeating geometry. It can also be noted that the finite element model is constructed with graded meshes, which can reduce the computational time without affecting model accuracy. Graded meshes typically have finer elements close to the high stress gradient zone.

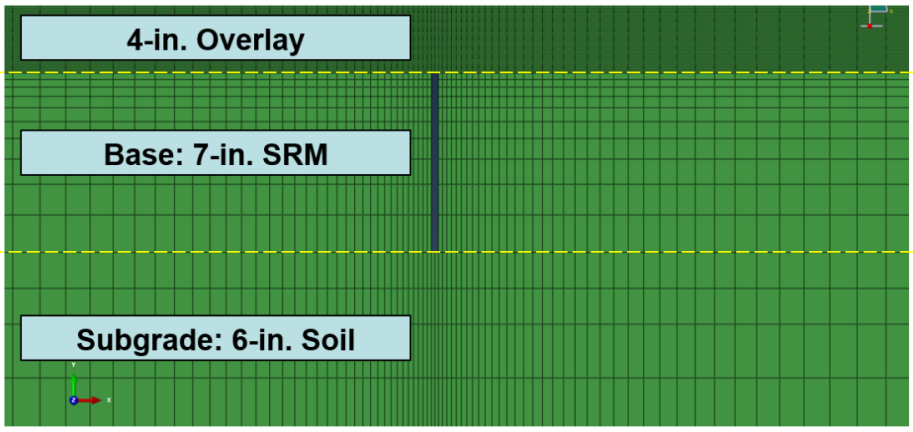

Figure 4.5. Selected pavement structure for FEM models.

The asphalt layer is cracked because of thermal and mechanical loading, and the crack is most likely developed from the top of the base layer because of high stress concentration. Therefore, cohesive zone elements are embedded through the asphalt overlay along the vertical line of the base joint for potential cracking due to thermal effects and/or mechanical truck loading, as shown in Figure 4.6.

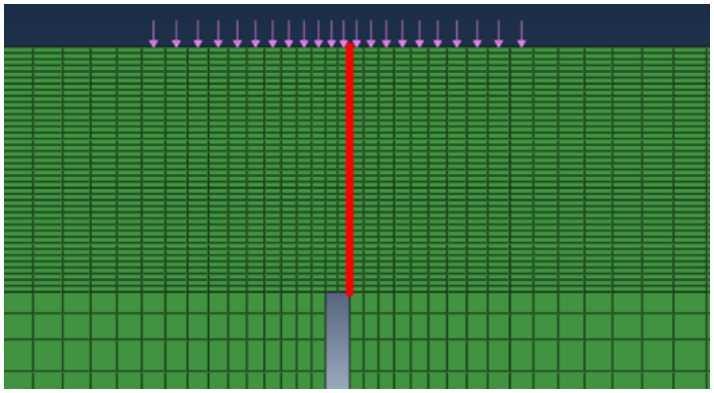

Figure 4.6. embedded cohesive elements (red vertical line).

The model for the new AC overlay is considered to be thermo-viscoelastic with cohesive zone fracture. Cohesive elements were predefined in this model and were embedded vertically from bottom to top of the overlay. For asphaltic base and soil as the subbase, thermo-viscoelastic and thermo-elastic models were considered respectively, noting that they are without damage or fracture. An average thermal expansion coefficient of the value 2.5E-5 was considered for overlay and base materials.

Six different rehabilitation alternatives were considered to study the thermal cracking behavior of asphalt overlay. For each case, two material qualities were used. (overall, 12 alternatives). Table 4.2 presents the cases and their geometric configurations.

Table 4.2 Rehabilitation Alternatives

Case	Description	Case	Description
I	4-inch SPR	IV	2-inch SPR + 2-inch SRM
II	1.5-inch SPR + 2.5-inch SRM	V	2-inch SLX + 2-inch SRM
III	1-inch SLX + 3-inch SRM	VI	4-inch SLX

4.3.2 Boundary conditions

As illustrated in Figure 4.7, both sides of the vertical edges were fixed in the horizontal direction, and the bottom of the mesh was fixed in the vertical direction, representing bedrock.

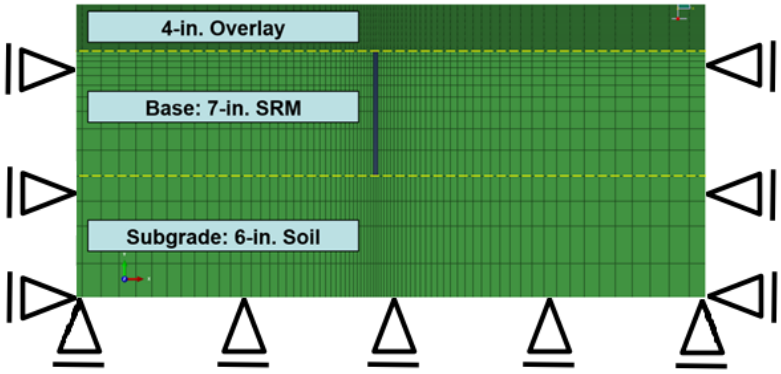

Figure 4.7. Schematic of the Boundary Conditions.

4.4 Loading

Two sets of loading have been applied on the pavement to assess its performance and cracking behavior. To analyze reflective cracking due to thermal loading, a temperature user-defined subroutine (UTEMP) was integrated with the analysis process. This subroutine was developed based on the spatial and temporal profile of the pavement, and the nodal value of temperature was calculated all over the domain. To apply mechanical loading, truck tire pressure was calculated and applied on the pavement surface.

4.4.1 Thermal loading

Thermal cracks in pavements often occur in a single, critical cooling event. Thus, prior to performing the thermal cracking simulation, the critical cooling events were researched from historical climate data. Temperature gradients with respect to the pavement depth for each pavement structure were estimated from the pavement surface temperature using an enhanced integrated climate model (EICM) developed by AASHTO.

According to the temperature data from 1995 to 2005 in Lincoln, Nebraska, it was found that the coldest temperature occurred in January of 2005. In that month, the air temperature dropped down to -22.1°C, and the average daily temperature change was -6°C. The critical temperature gradients and cooling cycles are shown in Figure 4.8.

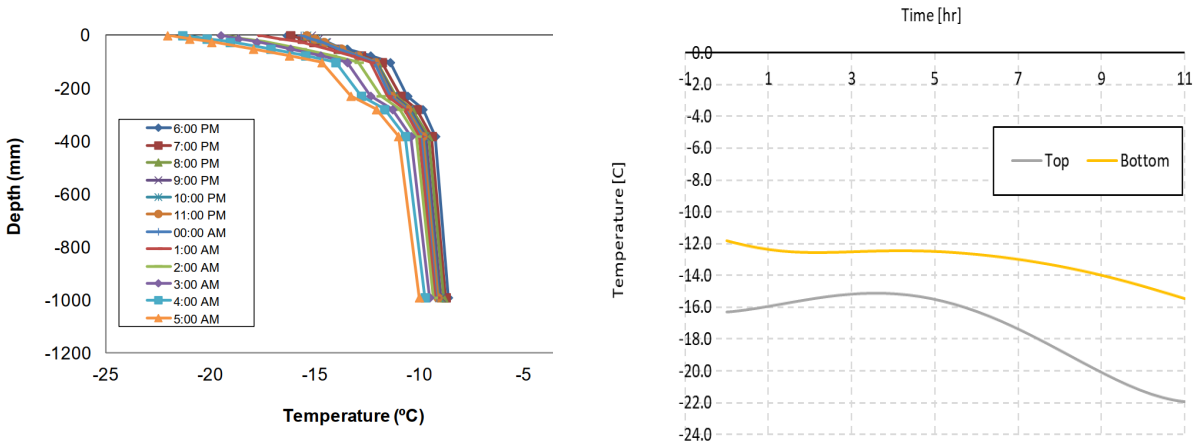

(a) (b)

Figure 4.8. Temporal and spatial temperature variation over, a) whole domain, and b) overlay.

As illustrated in the figure, the temperature of the pavement structure varies with pavement depth, depending on the underlying layers. In addition, the temperature variation with respect to time is significant at the surface, but it diminishes as the pavement depth increases.

Based on the temperature profiles presented in Figure 4.8, the time- and depth-dependent temperature profiles were implemented into the model through the user-defined temperature module (UTEMP). As observed in the figure, temperature decreases exponentially as depth increases. Thus, the temperature with depth, $T(h)$, was presented as an exponential function and each coefficient was related with time in the form of a fourth-order polynomial, as expressed by the following set of equations:

$$\begin{aligned} T(h) &= A_0(t) + A_1(t)[1 - \exp(-A_2(t).h)] \\ A_0(t) &= A_{00} + A_{01}t + A_{02}t^2 + A_{03}t^3 + A_{04}t^4 \\ A_1(t) &= A_{10} + A_{11}t + A_{12}t^2 + A_{13}t^3 + A_{14}t^4 \\ A_2(t) &= A_{20} + A_{21}t + A_{22}t^2 + A_{23}t^3 + A_{24}t^4 \end{aligned} \quad (4.8)$$

A least-squares-type error minimization was carried out to obtain the best-fitting model coefficients, which resulted in a coefficient matrix (3 by 5). A total of 15 coefficients would be sufficient to model the spatial and temporal temperature variations during the critical cooling

event. Figure 4.9 shows the temporal temperature variation at a specific location and how the polynomials are obtained.

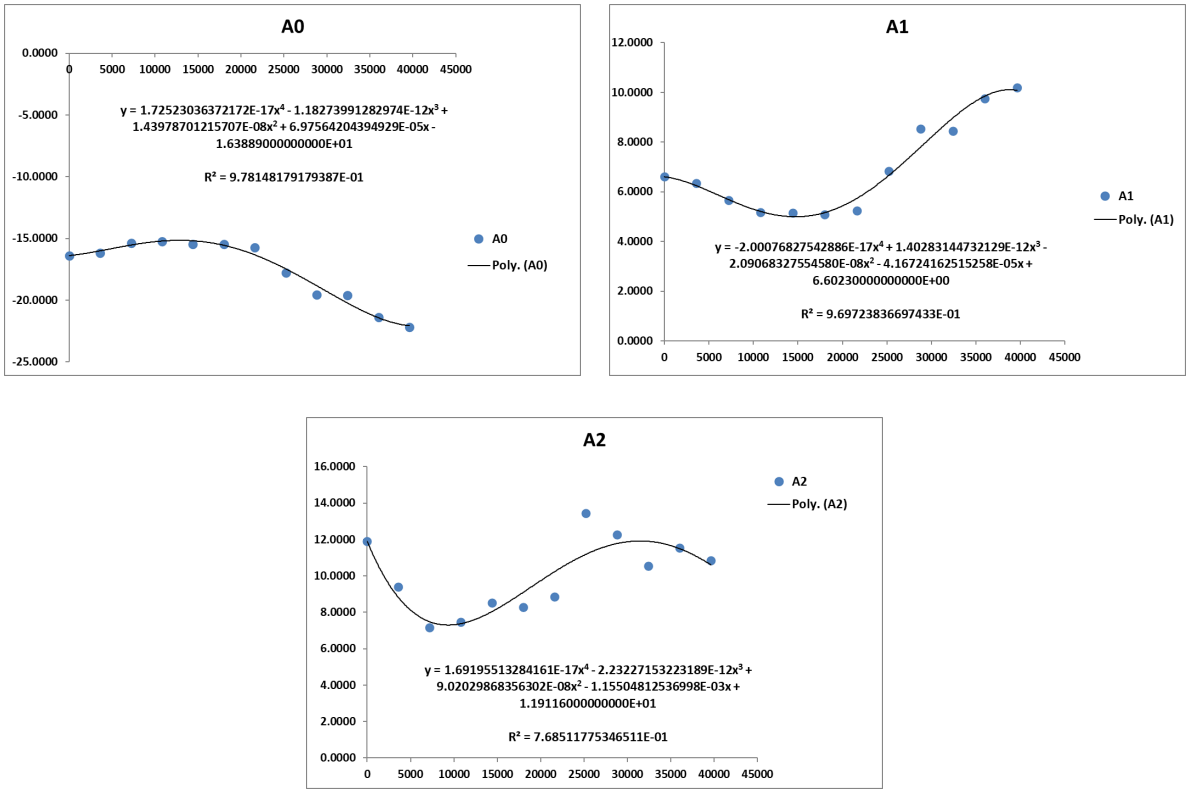

Figure 4.9. Temporal temperature variation at specific location.

4.4.2 Mechanical loading

To apply truck load on the pavement surface, loading configuration of a class 9 truck was used. To save time and to compare alternatives, a recurring trapezoidal loading pattern associated with pressure magnitude is used without rest periods. A total amount of 10,000 loading cycles were used for each alternative, and average stiffness degradation of the cohesive elements was calculated and considered as a criterion for pavement overlay crack resisting performance due to mechanical loads. Figure 4.10 shows the class 9 truck loading configuration.

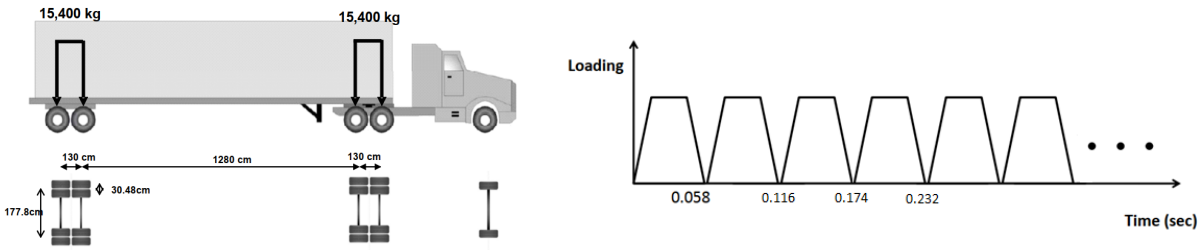

Figure 4.10. Mechanical load configuration.

4.5 Simulation results

In this subsection, the results of numerical simulation of pavement response to thermo-mechanical loading are discussed. First, thermal cracking in pavements using different rehabilitation alternatives is thoroughly examined. And then, reflective cracking due to mechanical loading is discussed.

4.5.1 Thermal cracking in pavements

Six cases and two material quality levels associated with them were modeled for temperature-induced thermal cracking. The results for each case are discussed as follows.

4.5.1.1 Case I (4-inch SPR)

Figures 4.11 (a) and (b) present the simulation results for the first case. As shown in the figures, although both good and poor-quality materials resisted the severe cooling event without failing, pavements with good-quality RAP lasted without the material yielding and experienced less tensile stress. The simulation results show that good-quality RAP could significantly reduce the tensile stress at the asphalt surface, while it did not change tensile stresses much at the bottom of the asphalt overlay. Although the asphalt overlay with the low quality material was performing worse, as illustrated in figure 4.11 (b), the pavement did not show thermal cracking, since the resulting tensile stress was lower than the critical stress state that causes material separation.

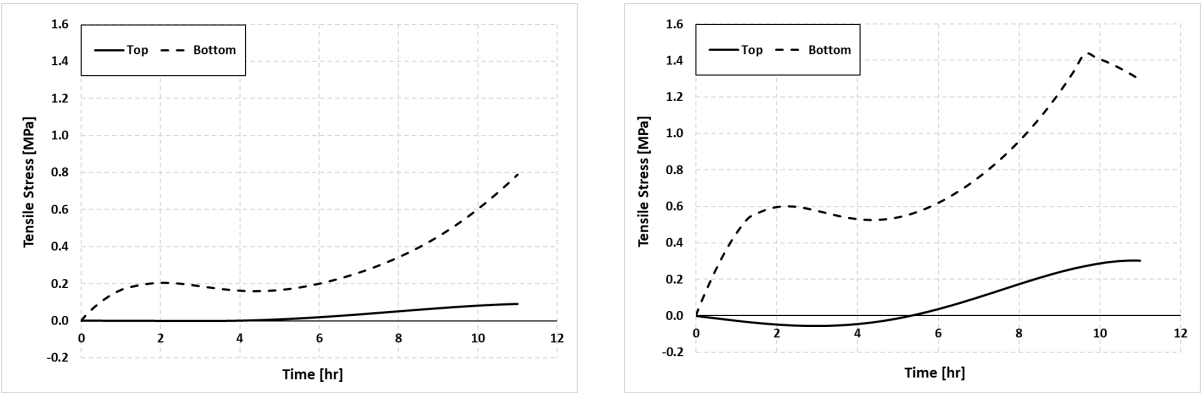

(a) (b)

Figure 4.11. Horizontal stresses at top and bottom of overlay in case I, using a) good-quality, and b) poor-quality material.

To observe the sensitivity of the model to overlay thickness, we used 2-inch overlay in the Case I FEM model. As can be seen in Figure 4.12, the pavement structure failed at 10th hour of the cooling event (around 4 am). From the simulation results, it can be concluded that the paving materials for rehabilitation practices and overlay thickness can significantly contribute to the thermally induced reflective cracking behavior.

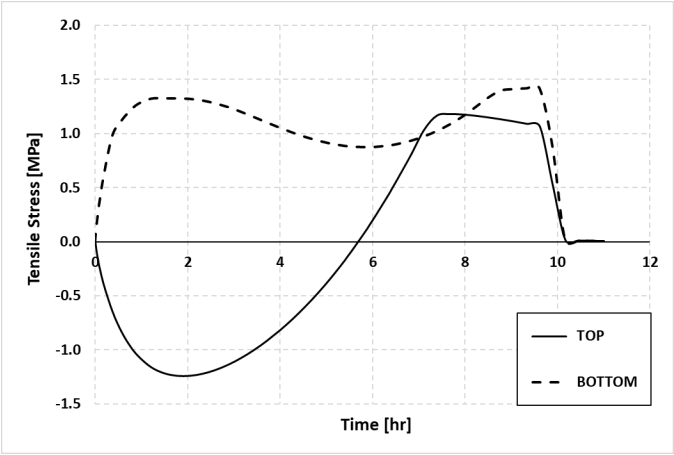

Figure 4.12. Horizontal stresses at top and bottom of overlay with 2-inch thickness.

4.5.1.2 Case II (1.5-inch SPR + 2.5-inch SRM)

As expected, the top part of the overlay which was filled with 1.5-inch SPR experienced less tensile stress in both poor-quality and good-quality material level as it was measured at the overlay surface and depicted in Figure 4.13. The bottom of the overlay, where 2.5-inch SRM was used experienced

more stress. It turned to be yielded at almost 10th hour of the cooling event (around 4am), when poor-quality material is used. The overlay with poor-quality material experienced comprehensive stress at almost three times that of its counterpart with good-quality material.

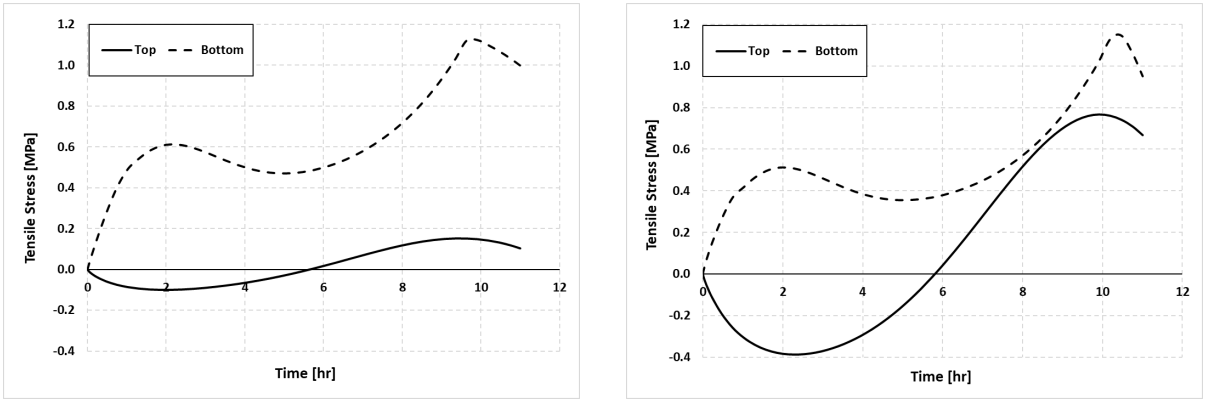

(a) (b)

Figure 4.13. Horizontal stresses at top and bottom of overlay in case II, using a) good-quality, and b) poor-quality material.

4.5.1.3 Case III (1-inch SLX + 3-inch SRM)

When 3-inch SRM and 1-inch SLX was used in the overlay, we expected to see an inferior performance due to high amount of SRM in the mix. As shown in Figure 4.14, the amount of maximum tensile stress that developed at the surface of the overlay was between 5 and 6 times more than the bottom of the overlay. Although the overlay did not fail, the bottom material yielded when poor-quality SRM was used. It features a steep slope in the figure meaning a huge drop in tensile stress after 9th hour of the cooling event. The result is shown in Figure 4.14.

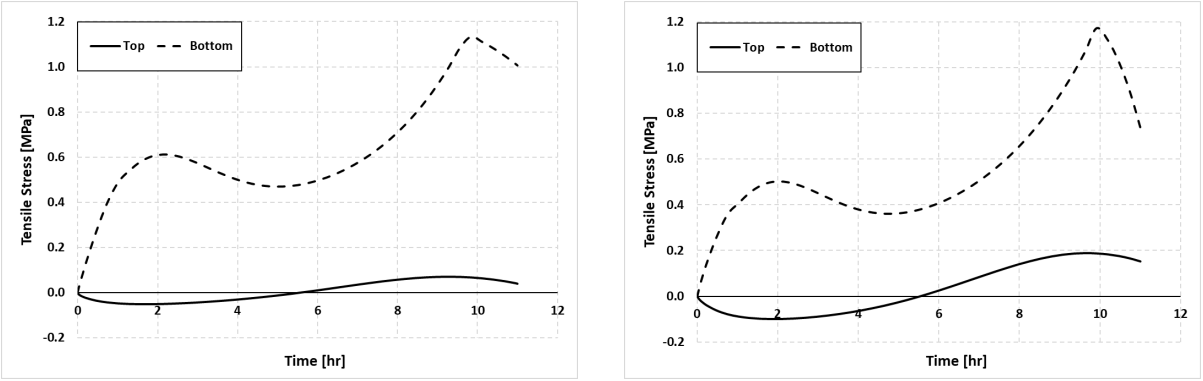

(a) (b)

Figure 4.14. Horizontal stresses at top and bottom of overlay in case III, using a) good-quality, and b) poor-quality material.

4.5.1.4 Case IV (2-inch SPR + 2-inch SRM)

As shown in Figure 4.15, One of the potential alternatives for rehabilitation practice, which is appealing because of its huge saving in construction costs is milling 4-inch of the overlay and filling it with 2-inch SRM at the bottom and 2-inch SPR on the top. The result of the simulation of thermal cracking for this case shows that both good and poor-quality materials resisted the severe cooling event. However, the stresses, both compressive and tensile, developed at the top and the bottom of the overlay were much higher in overlays with poor-quality material. In this case, slightly after the 8th hour of the cooling event, we saw almost equal tensile stress in the bottom and the top of the overlay. This behavior can also be seen in the second case where 1.5-inch SPR and 2.5-inch SRM were used. The similar damage behavior of the poor-quality SRM and SPR could lead to exhibiting this performance when the tensile stresses are accumulated due to variation of temperature in the overlay.

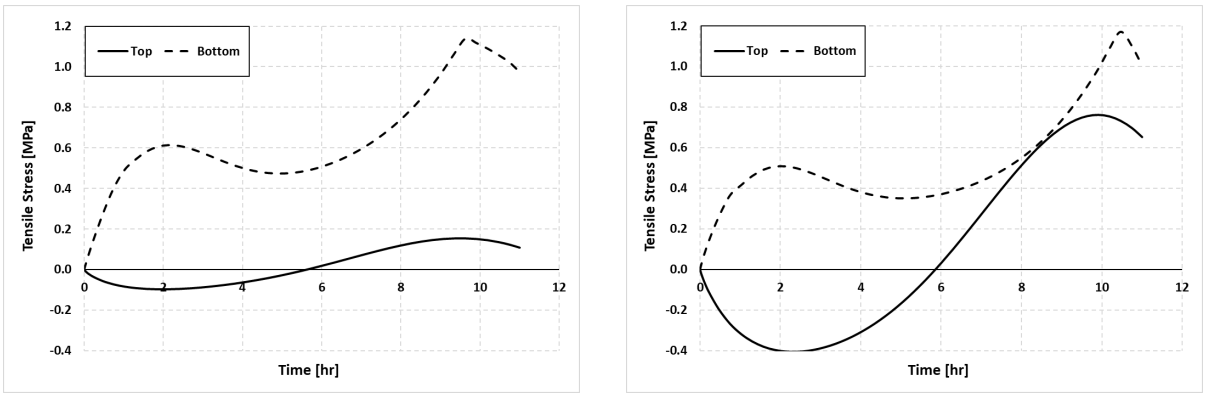

(a) (b)

Figure 4.15. Horizontal stresses at top and bottom of overlay in case IV, using a) good-quality, and b) poor-quality material.

4.5.1.5 Case V (2-inch SLX + 2-inch SRM)

The results of the simulation for this case is shown in Figure 4.16. As can be seen, this case exhibits almost the same thermal cracking behavior of case III, where only 1-inch SLX was used in the rehabilitation practice. Considering the cost of using SLX in construction of the overlay, the benefits of considering this case over the third case depends on their cracking behavior when mechanical loads are applied. The details of the simulated reflective cracking due to mechanical loads are discussed in the next sub-chapter.

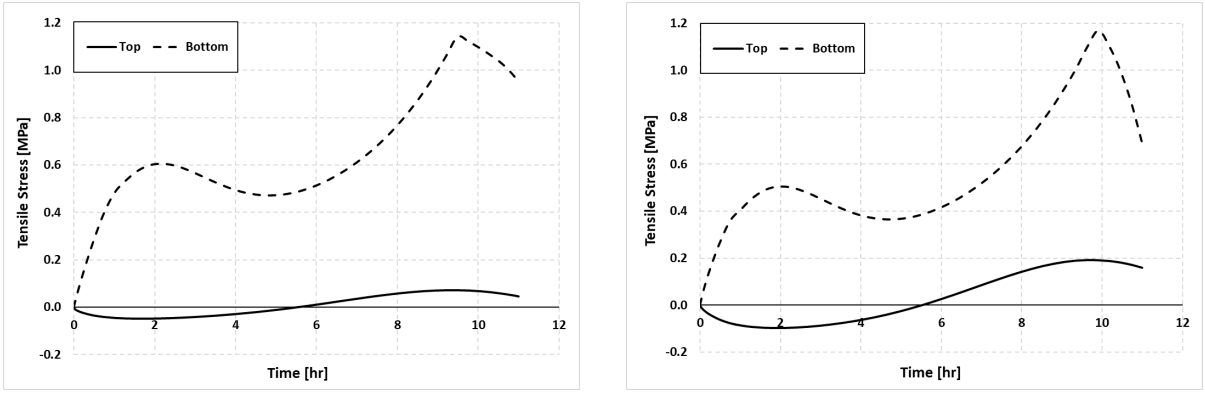

(a) (b)

Figure 4.16. Horizontal stresses at top and bottom of overlay in case V, using a) good-quality, and b) poor-quality material.

4.5.1.6 Case VI (4-inch SLX)

This case is the most expensive practice compared to the other alternatives in term of initial construction. The stresses developed in the overlay due to temperature variation was measured considering SLX material damage behavior at both the top and the bottom of the overlay. The results are shown in Figure 4.17. As expected, the poor-quality material performs worse than the good-quality material-built overlay. It also exhibited slightly more tensile stress at the bottom of the overlay compared to the other cases where SLX material were used. However, at good-quality material level, it shows superior performance compared all other rehabilitation alternatives.

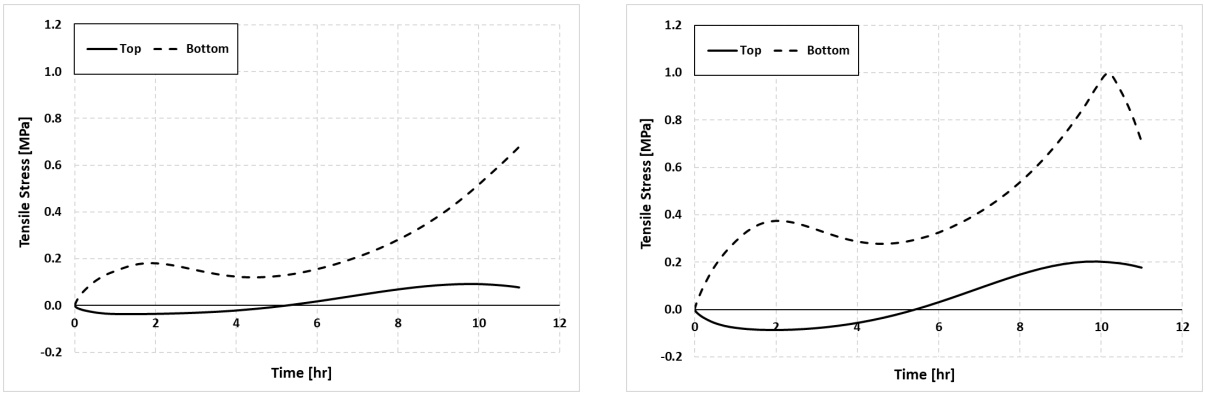

(a) (b)

Figure 4.17. Horizontal stresses at top and bottom of overlay in case VI, using a) good-quality, and b) poor-quality material.

4.5.1.7 Comparison of thermal cracking behavior in cases

The thermal cracking behavior of all the cases were compared and are shown in Figure 4.18. The behavior of the overlay at the top of the surface for all cases are depicted in Figure 4.18 (a), and the behavior for the bottom of the overlay is shown in Figure 4.18 (b). As noted for the bottom of the overlay, when we used good-quality materials, only case I (4-inch SPR) and case VI (4-inch SLX) resisted yielding, and the other cases with combinations of SRM with SLX and SPR yielded during the cooling event. However, none of them failed. When poor-quality materials were used in filling the overlay for rehabilitation purposes, all of the cases yielded at the bottom part. For the surface of the overlay, thermal cracking analysis results shows that the amount of tensile stress significantly increased for all of the cases as the material quality level dropped. Although, no

failure at top and bottom of the overlay was seen in all cases, we introduced a factor to compare their crack resisting behavior.

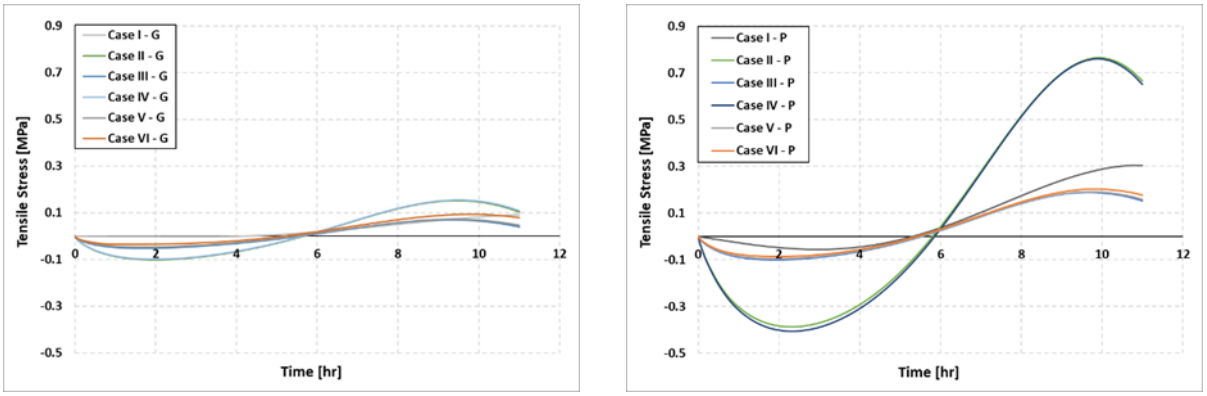

(a)

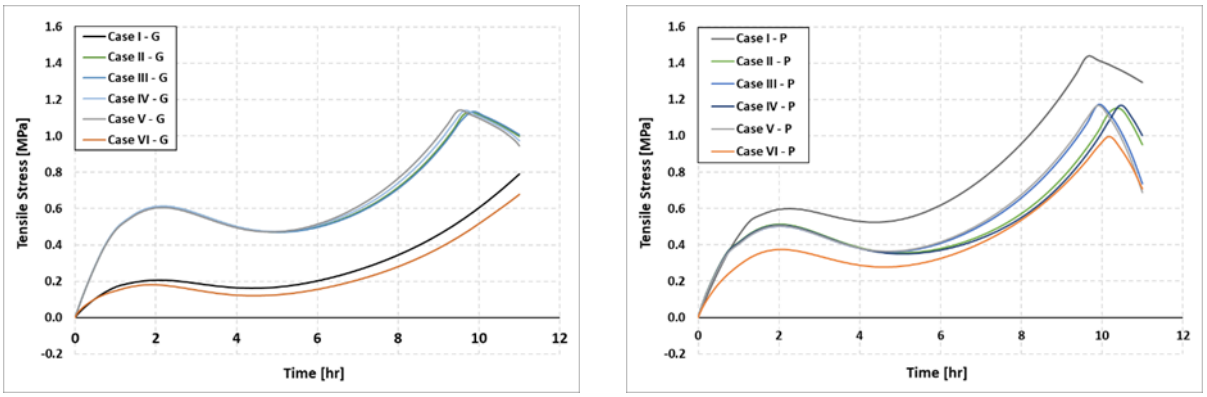

(b)

Figure 4.18. Thermal cracking behavior of pavements with different overlay configuration, a) top of the overlay, and b) bottom of the overlay.

If we calculate the area under the stress-time curve for the tensile part of the behavior of each case, as shown in Figure 4.19, we can calculate a term similar to the stored energy in concept. The more energy absorbed in the overlay, the closer it gets to the critical failure energy. Therefore, the alternatives can be ranked by their top surface energy storing behavior. Table 4.3 represents the amount of energy absorbed in each rehabilitation alternatives during critical cooling event.

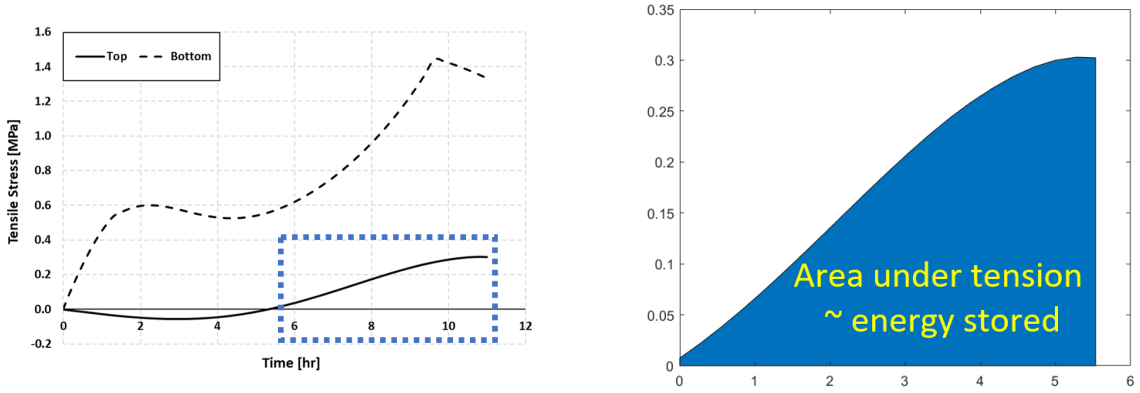

Figure 4.19. calculation the area under the tensile stress-time to evaluate pavement TC resistance.

Table 4.3 Energy absorbed in pavement overlay

Case		Stored tension energy (Top of the overlay)	Stored tension energy (Bottom of the overlay)
Case I	Good	0.2162	3.1555
	Poor	0.9899	8.3733
Case II	Good	0.5389	7.0599
	Poor	2.6408	5.9366
Case III	Good	0.2300	7.0249
	Poor	1.6236	6.1763
Case IV	Good	0.5418	7.1226
	Poor	2.4828	5.8459
Case V	Good	0.2631	7.1643
	Poor	1.1397	6.2154
Case VI	Good	0.2041	2.625
	Poor	0.6772	4.9569

To compare the increase in absorbed energy within the overlay with respect to case I (with 4-inch SPR), the results are depicted in Figure 4.20.

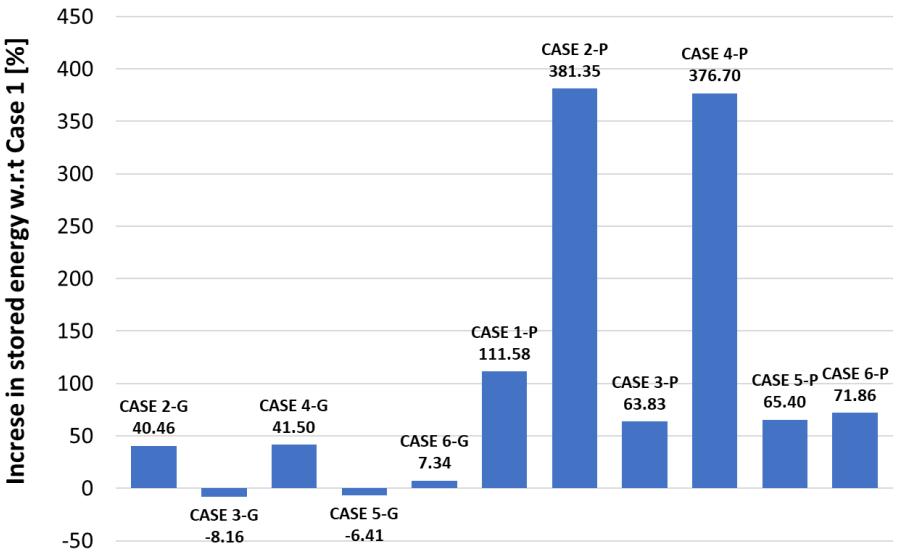

(a)

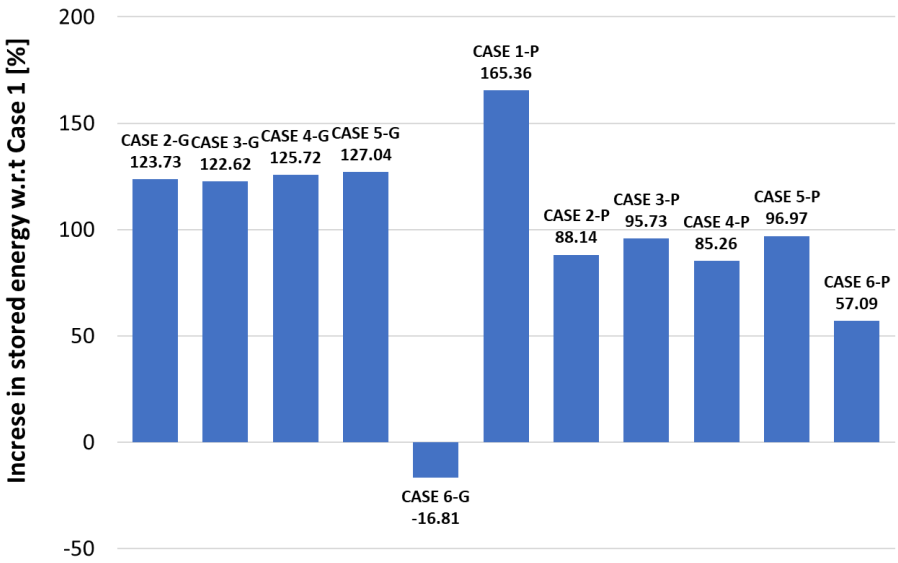

(b)

Figure 4.20. Increase in the absorbed energy within the overlay structure with respect to case 1: a) top of the overlay, and b) bottom of the overlay.

4.5.2 Mechanical Loading

In this section, the behavior of all six rehabilitation alternatives with good- and poor-quality RAP when mechanical load is applied on the surface of the overlay are discussed. The total number of 10,000 loading cycles were applied on each FEM model to compare their reflective cracking behavior. It should be noted that the reflective cracking analysis is a huge time-consuming process even using high-end computers. This number of loading cycles (10,000) take almost 48 hours for each case to be analyzed using 10-cores 2.4 GHz CPUs.

As discussed earlier in this chapter, the damage in the overlay was simulated using cohesive elements embedded in the FE model with a bilinear damage model associated with it. To obtain damage properties in the material level, SCB tests were conducted and the damage parameters for each case were calibrated and used in their FEM model. As the number of loading cycles increased, the damage accumulated in cohesive elements was measured and divided by the total number of cohesive elements in the FE model (which was considered same for all cases). The calculated results exhibited the extent of reflective cracking damage in each case due to mechanical loading. Table 4.4 represents the damage in cohesive elements. For each case, the damage in overlays made with poor-quality materials are marked with *.

Table 4.4 Accumulated reflective cracking damage in each case

Case		Damage in Cohesive Elements (%)
Case I	4-in. SPR	0.172583
		0.23103*
Case II	1.5-in. SPR + 2.5-in. SRM	0.195649
		0.25786*
Case III	1-in. SLX + 3-in. SRM	0.200096
		0.241748*
Case IV	2-in. SPR + 2-in. SRM	0.1878
		0.2493*
Case V	2-in. SLX + 2-in. SRM	0.183981
		0.23481*
Case VI	4-in. SLX	0.177251
		0.223153*

To get an insight on the behavior of each case when mechanical loads are applied, their total damage per loading cycles are depicted in Figure 4.21. As expected, the curves are showing almost linear trends beacause of the low number of loading cycles applied. The small extent of damage in each case (less than 1%) reflects this fact that the overlays are functioning in their healthy condition zone. We expected to see the nonlinear trend in damage behavior of the overlays if the number of loading cycles gets sufficiently high (it may take hundreds of thousand cycles). In that situation, we expect to see a plato zone after a certain number of loading cycles and another sharp increase in damage accumulated until the overlay fails.

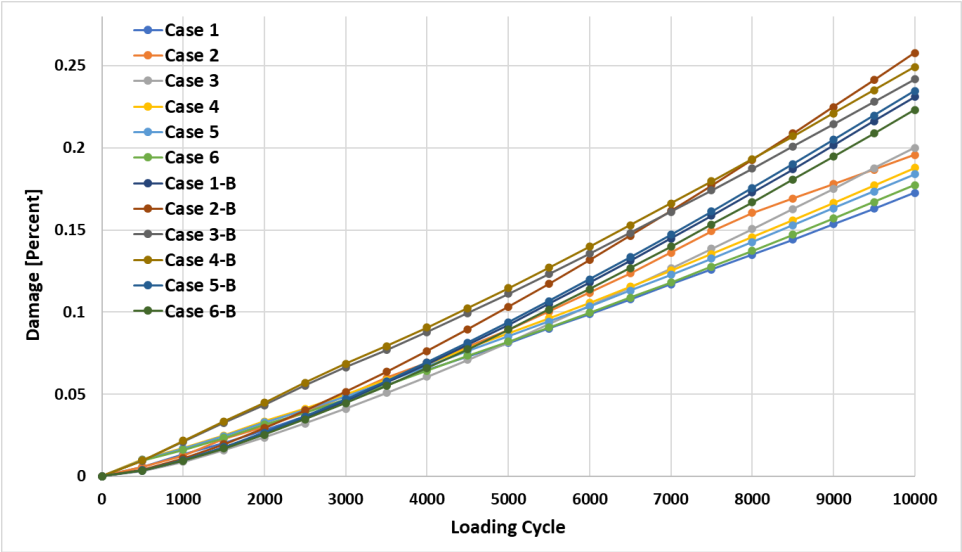

Figure 4.21. Reflective cracking damage per loading cycle in cases.

Figure 4.22 shows the increase in damage extent in all of the rehabilitation alternatives with respect to case I (4-inch SPR). As can be seen, the overlays made with poor-quality materials show significant damage increase compared to those made with good-quality materials.

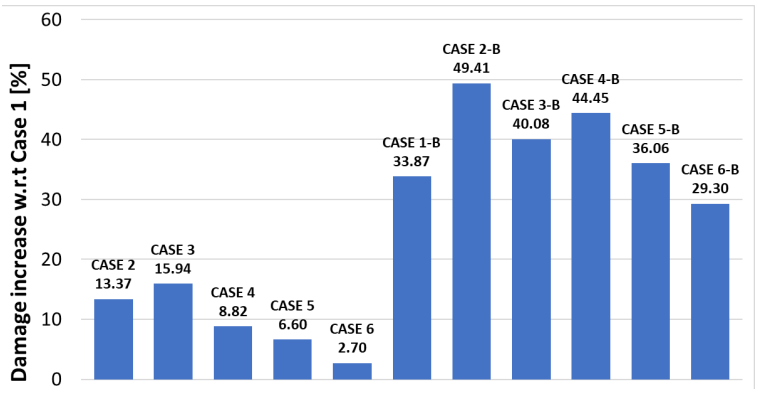

Figure 4.22. Damage increase with respect to the case I (4-inch SPR).

The poor-quality materials in the first case (4.0-in SPR) led to an increase in damage up to 34% with respect to its good-quality counterpart. The combination of 2.5-in. SRM and 1.5-in. SPR resulted in 13.4% more damage compared to 4-in. SPR. The reason behind this performance loss is the usage of SRM which has lower damage resistance capacity compared to other used materials.

The combination of 3.0-in. SRM and 1.0-in. SLX resulted in 16% more damage compared to 4-in. SPR. We see a slightly higher damage regardless of using a half inch more SRM in overlay, with respect to case II. This negligible change is because of the superior SLX quality and its damage performance. For the 4th case, the combination of 2.0-in. SRM and 2.0-in. SPR, the results show 8.8% more damage compared to 4-in. SPR while in the poor-quality case it increases up to 44.5%. The drastic change in damage performance showcases the low performance level in poor-quality RAP materials. Case V, which is made of 2-inch SRM and 2-inch SLX, shows 6.6% damage increase. The last case, in which 4-inch SLX was used in rehabilitation practice, performed very similar to the first case with 4-inch SPR. We expected to see an enhancement in reflective cracking behavior and less damage in pavement. However, it should be noted that some errors in material properties testing and calculation and in computational modeling of the pavements is inevitable. Looking at the linear fracture mechanism and a predefined cracking pattern could also have contributed to this 2% damage increase in case VI.

Chapter 5 Life Cycle Cost Analysis of Pavements

The life cycle cost analysis (LCCA) of each pavement structure was conducted to investigate the economic benefits of each rehabilitation practices. An LCCA tool developed by the Federal Highway Administration (FHWA), called RealCost 2.5 (FHWA 2010), was used in this study. Major inputs, the activities of each alternative, and assumptions made for the LCCA are summarized in Table 5.3. To achieve more realistic analysis, we used real input values (such as the construction cost, typical maintenance cost, traffic data, and work hours/duration) provided by NDOT. The maintenance frequency for each alternative in calculated based on their estimated structural life. To do this estimation, a linear extrapolation of damage-loading cycle behavior was done for each case to determine the number of loading cycles which lead to the overlay structural failure. It should be noted that thermal cracking behavior was not considered in the life estimation calculations. Then, using the traffic data provided by NDOT, the structural life for each case was estimated in years, as represented in Table 5.1. The process is depicted in Figure 5.1.

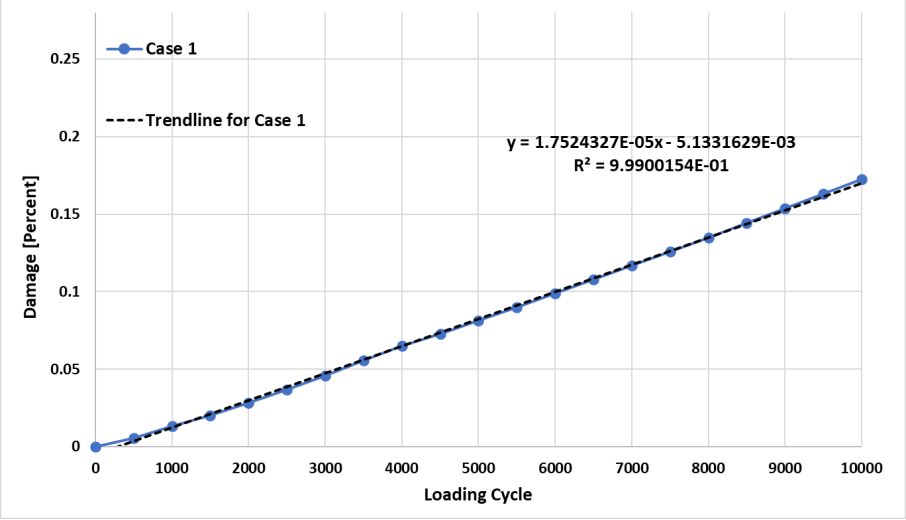

Figure 5.1. Estimation of structural life based on linear extrapolation.

$$y = 1.7524327 \times 10^{-5}x - 5.1331629 \times 10^{-3}$$

$$\xrightarrow{y=100} x = 5706645 \text{ (number of loading cycles leads to failure)}$$

$$\frac{x = 5706645}{ADTT = 700} \times \frac{1\ year}{365\ days} = 22.34\ years$$

where,

y = damage extent in percent

x = number of cycles

Table 5.1 Estimated structural life for each case

Cases	Estimated life (in years)
4-inch SPR	22.33521
	16.41708*
1.5-inch SPR + 2.5-inch SRM	19.04088
	14.70926*
1-inch SLX + 3-inch SRM	18.94948
	16.24067*
2-inch SPR + 2-inch SRM	20.93204
	15.74872*
2-inch SLX + 2-inch SRM	21.36648
	16.15283*
4-inch SLX	22.18101
	16.9965*

Although there is great variability in preventive maintenance strategies depending on the location of the projects, Nebraska DOT suggests the maintenance strategy as follows.

Table 5.2 Maintenance strategy suggested by NDOT

Activity timeline	Maintenance activity	Operation cost ($1000)
At 25% of life	armor coat / chip seal / expanded shale	29.0 / 33.0 / 43.0
At 25% of life	crack seal	13.0
At 50% of life	crack seal	13.0
At 75% of life	armor coat / chip seal / expanded shale	29.0 / 33.0 / 43.0
At 75% of life	crack seal	13.0

Two different locations as shown in Figure 5.2, and their traffic volume were selected for LCCA based on annual average daily traffic counts in the state of Nebraska.

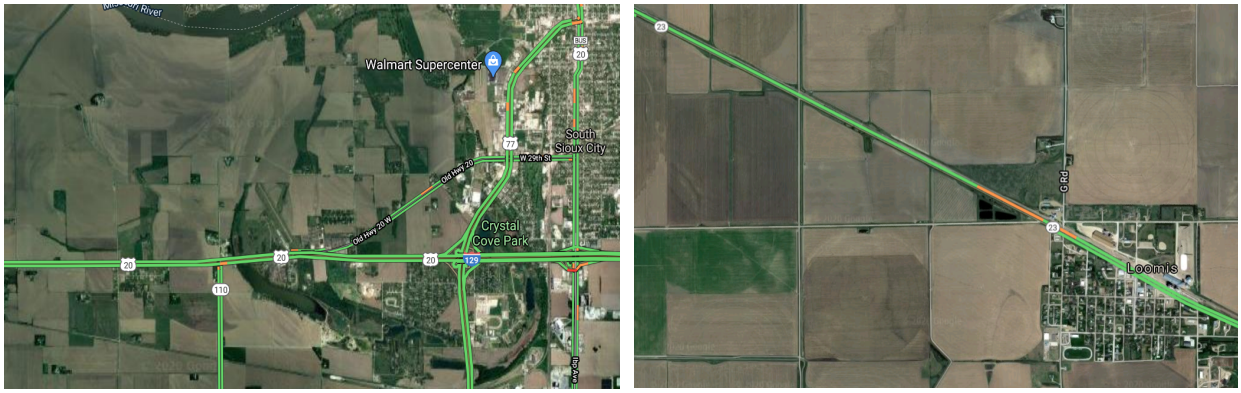

(a) (b)

Figure 5.2. High (a) and low (b) traffic zones selected for LCCA: a) West Jct N9 to Jackson on US-20 and b) Bertland-Loomis on N23.

It was assumed that the maintenance period after the first maintenance operation would be 25% and 50% of the overlay structural life for minor and major activities, respectively. The average six alternatives were evaluated in this study: case I through case VI at low- and high-volume traffic conditions for a total 45-year analysis period. With the given traffic condition, the structural life of each alternative was estimated and presented in Table 5.1. Since each project is differentiated by only the rehabilitation practice (six cases with good-quality material) and its expected service life, for the sake of simplicity, the construction/rehabilitation duration and the traffic data were considered similar for all cases. However, using a range of values for input data depending on low/high traffic volume enabled us to do a probabilistic analysis as well. Table 5.3 represents the input data for LCCA.

Table 5.3 Input for LCCA of rehabilitation practices for 45 years analysis period

Alternative 1				
Estimated life	**No. of activities**	**Work duration (days)**	**Maintenance frequency (years)**	**Construction cost ($/1-mile)**
22.34	8	0.3	5.5 / 11	228048.558
Alternative 2				
19.04	9	0.3	5 / 10	216509.212
Alternative 3				
18.95	9	0.3	5 / 10	220967.736
Alternative 4				
20.93	9	0.3	5 / 10	220729.981
Alternative 5				
21.37	8	0.3	5.5 / 11	237723.767
Alternative 6				
22.18	8	0.3	5.5 / 11	261671.330

Traffic Input		
Parameters	**High Traffic volume**	**Low Traffic volume**
AADT construction year (total)	8215	1460
Total trucks as percentage of AADT (%)	24	13
Annual growth rate of traffic	1.1	0.6
Speed limit under normal condition (mph)	65	55
Work zone speed limit (mph)	50	40
Discount rate (%)	2.0	
Value of time for passenger cars ($/hour)	13.96	
Value of time for single unit trucks ($/hour)	22.34	
Value of time for combination trucks ($/hour)	26.89	

Table 5.4 presents the deterministic LCCA results for high traffic volume route. Both the agency costs and user costs of each alternative are summarized in terms of net present value and equivalent uniform annual cost (EUAC). As shown in the table, the SPR-overlay pavement

resulted in lower agency costs, and the SLX-overlay had the lowest user costs at high traffic conditions. The analysis results clearly support the benefits of using 4-inch SPR for rehabilitation purpose because of its: 1) lower maintenance frequency, 2) lower need for major maintenance activity, and 3) longer service life.

Table 5.4 Deterministic LCCA results for high traffic condition

Cases	Costs ($1000)	Undiscounted sum ($1000)	Present Value ($1000)	EUAC ($1000)
Case I	User	217.03	211.14	7.16
	Agency	419.78	349.71	11.86
Case II	User	219.33	212.66	7.21
	Agency	448.81	361.63	12.26
Case III	User	219.46	212.84	7.22
	Agency	453.92	368.76	12.50
Case IV	User	218.83	212.25	7.20
	Agency	446.93	362.29	12.29
Case V	User	217.15	211.21	7.16
	Agency	431.63	360.43	12.22
Case VI	User	216.99	211.06	7.16
	Agency	452.53	382.67	12.98

The expenditure stream for agency cost at high traffic volume condition was considered for initial construction and regular maintenance for each case based on their service life. It is represented in Figure 5.3. Present value of agency costs are shown in Figure 5.4.

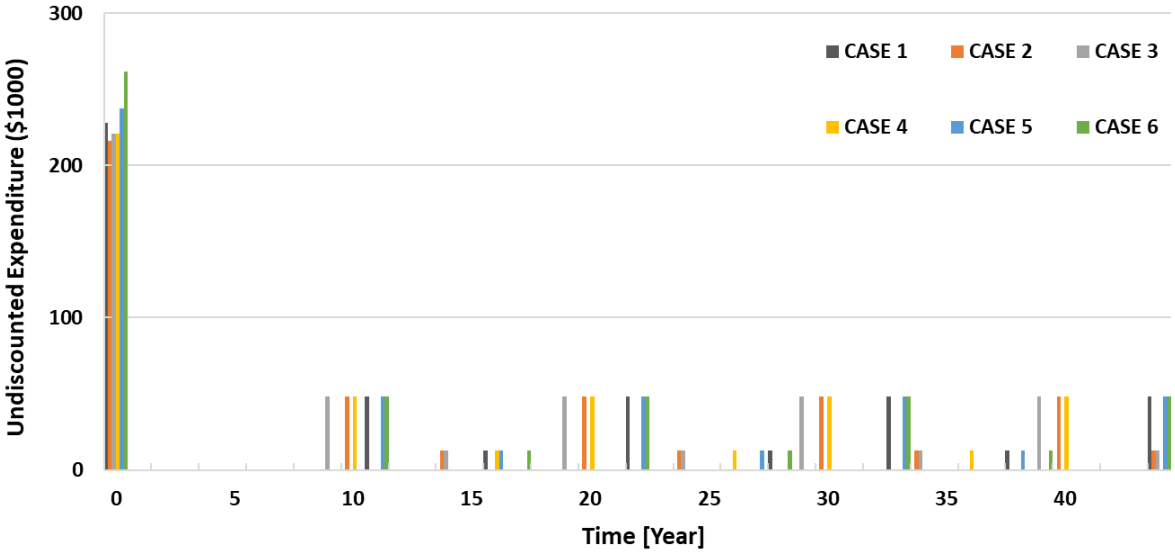

Figure 5.3. Expenditure stream for agency cost at high traffic volume condition.

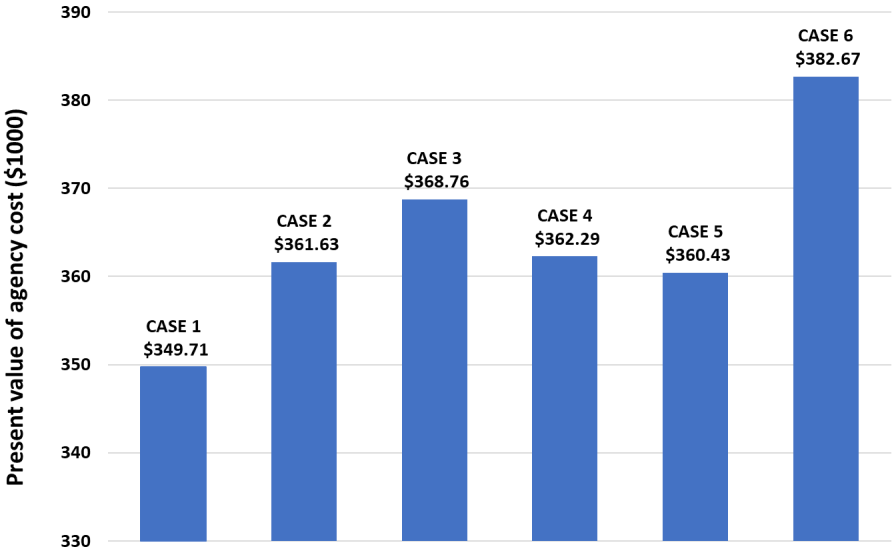

Figure 5.4. Present value of agency cost at high traffic condition.

Chapter 6 Summary and Conclusions

To improve pavement engineering practices in Nebraska, the feasibility and potential applications of alternative overlay configurations with RAP were studied. To address important questions regarding the performance of different rehabilitation alternatives and their economic benefits, a fully mechanistic approach was used to analyze the pavement performance when thermal and mechanical loads were applied. Then, the LCCA of each alternative was examined to compare them to the conventional 4-inch mill and fill rehabilitation practice using SPR mixture. The rehabilitation alternatives considered in this project were: 4.0-inch SPR (a reference case), 1.5-inch SPR + 2.5-inch SRM, 1.0-inch SLX + 3.0-inch SRM, 2.0-inch SPR + 2.0-inch SRM, 2.0-inch SLX + 2.0-inch SRM, and 4.0-inch SLX. Each alternative was considered with two mixture quality levels by incorporating two different RAPs: good and poor, which led to total 12 different cases.

Two laboratory tests (i.e., dynamic modulus test and SCB fracture test) were conducted, and test results were integrated with mixture finite element modeling to identify mixture properties. The resulting mixture properties were used to conduct pavement performance model simulation with a finite element method. Pavement simulation results were then used for the LCCA to examine the long-term economic benefits of each rehabilitation alternative compared to the conventional rehabilitation practice (i.e., 4-inch SPR). The following bullet points summarize the conclusions drawn from this research project:

- SLX showed a little more ductile and better fracture resistance than SPR and SRM.
- In terms of load-induced reflective cracking, pavement performance simulation results showed that the conventional overlay practice with the SPR mixture would perform similar with the case of 4.0-in. SLX and generally better than other cases considered in this study.
- In terms of thermally-induced cracking, pavement performance simulation results showed that the case with 4-in. SLX was the best, and cases with SLX on top generally perform better than cases with SPR.
- The overlays made with poor-quality RAP showed significant damage increase compared to those made with good-quality RAP. This implies a careful use and management of RAP is desired to sustain long-term pavement performance.

- LCCA based on reflective cracking results indicated that the 4.0-in. SPR (Case I) is the most economical strategy compared to other alternatives considered in this study in terms of the agency costs.
- It can be noted that the combination of 2-inch SRM + 2-inch SLX is a good option for colder regions in Nebraska, as the combined overlay showed almost similar reflective cracking behavior to and better in thermal cracking resistance than the conventional 4.0-in. SPR rehabilitation.
- For future studies, it is recommended to use a finite element modeling which couples thermo- and mechanical behavior to predict the concurrent effects of temperature and truck loads on pavement performance.

References

AASHTO TP 62-07. (2008). Determining dynamic modulus of hot-mix asphalt concrete mixtures. *Standard Specifications for Transportation and Methods of Sampling and Testing, 28th Edition, and Provisional Standards*. America Association of State Transportation and Highway Engineering.

Abaqus (2014). *User's Manual Version 6.10*. Providence, RI: Habbit, Karlsson and Sorensen, Inc.

Aragão, F. T. S. (2011). Computational microstructure modeling of asphalt mixtures subjected to rate-dependent fracture. Ph.D. Dissertation, University of Nebraska, Lincoln.

Aragão, F. T. S., & Kim, Y. R. (2012). Mode I fracture characterization of bituminous paving mixtures at intermediate service temperatures. *Experimental mechanics*, *52*(9), 1423-1434.

Aurangzeb, Q., & Al-Qadi, I. L. (2014). Asphalt pavements with high reclaimed asphalt pavement content: Economic and environmental perspectives. In *Transportation Research Record* (pp. 161-169). (Transportation Research Record; Vol. 2456). National Research Council. https://doi.org/10.3141/2456-16

Baek, J., & Al-Qadi, I. (2009). Reflective cracking: Modeling fracture behavior of hot-mix asphalt overlays with interlayer systems. *Asphalt Paving Technology-Proceedings, 28*, 789-824.

Ban, H., Im, S., & Kim, Y.-R. (2013). Nonlinear viscoelastic approach to model damage associated performance behavior of asphaltic mixture and pavement structure. *Canadian Journal of Civil Engineering, 40*(4), 313-323.

Bazant, Z. P. & Planas, J. (1998). *Fracture and size effect in concrete and other quasibrittle materials*. Boca Raton, FL: CRC Press LLC.

Darabi, M. K., Al-Rub, R. K. A., Masad, E. A., & Little, D. N. (2013). Constitutive modeling of fatigue damage response of asphalt concrete materials with consideration of microdamage healing. *International Journal of Solids and Structures, 50*(19), 2901-2913.

Darabi, M. K., Al-Rub, R. K. A., Masad, E. A., Huang, C. W., & Little, D. N. (2011). A thermo-viscoelastic–viscoplastic–viscodamage constitutive model for asphaltic materials. *International Journal of Solids and Structures*, *48*(1), 191-207.

Darabi, M. K., Al-Rub, R. K. A., & Little, D. N. (2012). A continuum damage mechanics framework for modeling micro-damage healing. *International Journal of Solids and Structures*, *49*(3-4), 492-513.

Dave, E. V., Song, S. H., Buttlar, W. G., & Paulino, G. H. (2007). Reflective and thermal cracking modeling of asphalt concrete. *Proceedings of the Advanced Characterization of Pavement and Soil Engineering Materials*, Athens, Greece, 1241-125.

Dave, E. V. & Buttlar, W. G. (2010). Thermal reflective cracking of asphalt concrete overlays. *International Journal of Pavement Engineering, 11*(6), 477-488.

Duan, K., Hu, X., & Wittmann, F. H. (2006). Scaling of quasi-brittle fracture: boundary and size effect. *Mechanics of Materials, 38*, 128-141.

Espinosa, H. D. & Zavattieri, P. D. (2003). A grain level model for the study of failure initiation and evolution in polycrystalline brittle materials, part I: theory and numerical implementation. *Mechanics of Materials, 35*, 333-364.

FHWA (2010). Life-Cycle Cost Analysis - RealCost Use Manual. National Center for Pavement Preservation Foundation for Pavement Preservation (FHWA).

Geubelle, P. & Baylor, J. (1998). Impact-induced delamination of laminated composites: a 2D simulation. *Composites Part B – Engineering, 29*(5), 589-602.

Guthrie, W. S., & Butler, M. J. (2011). Field evaluation of asphalt overlays on state route 30 in Northern Utah. *Proc., 90th Annual Meeting of the Transportation Research Board, Washington, DC*, Transportation Research Board.

Hoare, T. R. & Hesp, S. (2000). Low-temperature fracture testing of asphalt binders: regular and modified systems. *Transportation Research Record, 1728*, 36-42.

Hoerner, T. E., K. A. Zimmerman, K. D. Smith, and L. Allen Cooley, Mechanistic-Empirical Pavement Design Guide Implementation Plan, Final Report No. SD2005-01, Applied Pavement Technology, South Dakota Department of Transportation, Pierre, South Dakota, October 2007, 312 p.

Im, S., Kim, Y.-R., & Ban, H. (2010). Layer moduli of Nebraska pavements for the new mechanistic-empirical pavement design guide (MEPDG). Report No. MPM-08, University of Nebraska-Lincoln, Department of Civil Engineering, Lincoln, NE.

Im, S., You, T., Ban, H., & Kim, Y. -R. (2015). Multiscale testing-analysis of asphaltic materials considering viscoelastic and viscoplastic deformation. *International Journal Of Pavement Engineering* (http://dx.doi.org/10.1080/10298436.2015.1066002)

Johanneck, L., Clyne, T., Tompkins, D., & Khazanovich, L. (2011). Evaluation and Local Calibration of MEPDG EICM Model Using MnRoad Data. *Proc., 90th Annual Meeting of the Transportation Research Board, Washington, DC*, Transportation Research Board.

Khazanovich, L., Tompkins, D., Wu, R., & Harvey, J. (2013). Investigation and modification of available mechanistic-empirical procedures for reflective cracking in asphalt overlays of concrete pavements. *Transportation Research Record: Journal of the Transportation Research Board, 2368,* 126-132.

Khosla, N. P., & Visintine, B. (2011). Effect pf the Use of Higher Percentages of RAP in NCDOT Hot Mix Asphalt.

Kim, H., Wagoner, M. P., & Buttlar, W. G. (2008). Simulation of fracture behavior in asphalt concrete using a heterogeneous cohesive zone discrete element model. *Journal of Materials in Civil Engineering, 20*(8), 552-563.

Kim, H. & Buttlar, W. G. (2009). Finite element cohesive fracture modeling of airport pavements at low temperatures. *Cold Regions Science and Technology, 57*, 123-130.

Kim, Y. R., Allen, D. H., & Little, D. N. (2005). Damage-induced modeling of asphalt mixtures through computational micromechanics and cohesive zone fracture. *Journal of Materials in Civil Engineering*, *17*(5), 477-484.

Kim, Y. R., Allen, D. H., & Little, D. N. (2007). Computational constitutive model for predicting nonlinear viscoelastic damage and fracture failure of asphalt concrete mixtures. *International Journal of Geomechanics*, *7*(2), 102-110.

Lee, N. K., Morrison G. R., & Hesp, S. (1995). Low temperature fracture of poluethylene modified asphalt binders and asphalt concrete mixes. *Journal of the Association of Asphalt Paving Technologists, 64*, 534-574. 58

Li, X., & Marasteanu, M. O. (2004). Evaluation of the low temperature fracture resistance of asphalt mixtures using the semi-circular bend test. *Journal of the Association of Asphalt Paving Technologists, 73*, 401-426.

Li, X., & Marasteanu, M. O. (2010). The fracture process zone in asphalt mixture at low temperature. *Engineering Fracture Mechanics, 77*, 1175-1190.

Lutif, J. E., Souza, F. V., Kim, Y., Soares, J. B., & Allen, D. H. (2010). Multiscale modeling to predict mechanical behavior of asphalt mixtures. *Transportation research record*, *2181*(1), 28-35.

Marasteanu, M. O., Dai, S. T., Labuz, J. F., & Li, X. (2002). Determining the low-temperature fracture toughness of asphalt mixtures. *Transportation Research Record, 1789*, 191-199.

Marasteanu, M. O., Zofka, A., Turos, M., Li, X., Velasques, R., Buttlar, W., Paulino, G., Braham, A., Dave, E., Ojo, J., Bahia, H., Williams, C., Bausano, J., Gallistel, A., & McGraw, L. (2007). Investigation of low temperature cracking in asphalt pavements: national pooled fund study 776. *Final Report No. MN/RC 2007-43*, Minnesota Department of Transportation.

Mobasher, B., Mamlouk, M. S., & Lin, H. M. (1997). Evaluation of crack propagation properties of asphalt mixtures. *Journal of Transportation Engineering, 123*(5), 405-413.

Molenaar, A. A. A., Scarpas, A., Liu, X., &. Erkens, S. M. J. G. (2002). Semicircular bending test: simple but useful? *Journal of the Association of Asphalt Paving Technologists, 71*, 794-815.

Mukhtar, M. T., & Dempsey, B. J. (1996). Interlayer stress absorbing composite (ISAC) for mitigating reflective cracking in asphalt concrete overlays. *Final Report, Transportation Engineering Series No. 94*, Cooperative Highway and Transportation Series No. 260, University of Illinois, Urbana, IL.

Norouzi, M., Nassiri, S., Haghi, N. T., & Bayat, A. (2014). Performance evaluation of asphalt overlays in Alberta using long term pavement performance specific pavement study 5 sections. *International Journal of Pavement Research and Technology, 7*(1), 60.

Qiao, Y., Dawson, A., Parry, T., & Flintsch, G. (2019). Life cycle cost of flexible pavements and climate variability: case studies from Virginia. *Structure and Infrastructure Engineering*, *15*(12), 1665-1679.

Rodrigues, J. A., Teixeira, J. E. S. L., Kim, Y. R., Little, D. N., & Souza, F. V. (2019). Crack modeling of bituminous materials using extrinsic nonlinear viscoelastic cohesive zone (NVCZ) model. *Construction and Building Materials*, *204*, 520-529.

Seo, Y., Kim, Y. R., & Witczak, M. W. (2002). Application of the digital image correlation method to mechanical testing of asphalt-aggregate mixtures. *Transportation Research Record, 1789*, 162-172.

Shakiba, M., Gamez, A., Al-Qadi, I., & Little, D. N., (2017) Introducing realistic tire–pavement contact stresses into Pavement Analysis using Nonlinear Damage Approach (PANDA), *International Journal of Pavement Engineering, 18*(11), 1027-1038.

Slevadurai, A. P. S., Au, M. C., & Phang, W. A. (1990). Modeling of low-temperature behavior of cracks in asphalt pavement structures. *Canadian Journal of Civil Engineering, 17*, 844-858.

Song, S. H., Paulino, G. H., & Buttlar, W. G. (2006). A bilinear cohesive zone model tailored for fracture of asphalt concrete considering viscoelastic bulk material. *Engineering Fracture Mechanics*, 2829-2847.

Song, S. H., Wagoner, M. P., & Paulino, G. H. (2008). δ25 crack opening displacement parameter in cohesive zone models: experiments and simulations in asphalt concrete. *Fatigue and Fracture of Engineering Materials and Structures*, *31*, 850-856. 59

Souza, F. V., & Castro L. S. (2012). Effect of temperature on the mechanical response of thermo viscoelastic asphalt pavements. *Construction and Building Materials, 30*, 574-582.

van Rooijen, R. C., & de Bondt A. H. (2008). Crack propagation performance evaluation of asphaltic mixes using a new procedure based on cyclic semi-circular bending tests. *Pavement cracking: mechanisms, modeling, detection, testing, and case histories*, CRC Press, 437-446.

Wagoner, M. P., Buttlar, W. G., & Paulino, G. H. (2005). Disk-shaped compact tension test for asphalt concrete fracture. *Society for Experimental Mechanics, 45*(3), 270-277.

Wagoner, M. P., Buttlar, W. G., Paulino, G. H., & Blankenship, P. (2006). Laboratory testing suite for characterization of asphalt concrete mixtures obtained from field cores. *Journal of the Association of Asphalt Paving Technologists, 75*, 815-852.

Wang, Y. D., Ghanbari, A., Underwood, S., & Kim, Y. (2020). Development of Preliminary Transfer Functions for Performance Predictions in FlexPAVE™.

Williams, M. L., Landel, R. F., & Ferry, J. D. (1955). The temperature dependence of relaxation mechanisms in amorphous polymers and other glass-forming liquids. *Temperature Dependence of Relaxation Mechanisms*, 77(14), 3701-3707.

Wu, Z., Chen, X., Gaspard, K., & Zhang, Z., (2008). Structural overlay design of flexible pavement by non-destructive test methods in Louisiana. *Transportation Research Board Annual Meeting*, 08-1704.

You, T., Al-Rub, R. K. A., Darabi, M. K., Masad, E. A., & Little, D. N. (2012). Three-dimensional microstructural modeling of asphalt concrete using a unified viscoelastic–viscoplastic–viscodamage model. *Construction and Building Materials*, *28*(1), 531-548.

You, T., Masad, E. A., Al-Rub, R. K. A., Kassem, E., & Little, D. N. (2014). Calibration and validation of a comprehensive constitutive model for asphalt mixtures. *Transportation Research Record: Journal of the Transportation Research Board, 2447*(1), 13-22.

Zare, K., & Kim, Y. R. (2018). MIDAS-VT-Pre: Software to generate 2D finite element model of particle/fiber embedded composites with cohesive zones. SoftwareX 10, 100292.

Rami, K. Z., Kim, Y. R., Khedmati, M., Nsengiyumva, G., & Alanazi, H. (2018). Two-way linked multiscale method integrated with nanomechanical tests and cohesive zone fracture to model highly heterogeneous binding materials. Journal of Engineering Mechanics, 144(10), 04018095.

Zhou, C., Huang, B., Shu, X., & Dong, Q. (2013). Validating MEPDG with Tennessee pavement performance data. *American Society of Civil Engineers: Journal of Transportation Engineering*, 139(3).